Article

Neuron

Phosphodiesterase 10A Inhibition Improves Cortico-Basal Ganglia Function in Huntington's Disease Models

Highlights

- Q175 and R6/2 HD models exhibit reduced PDE10A equivalent to manifest HD patients
- PDE10 inhibition restored striatal input and indirect pathway output in HD mice
- Both cAMP and cGMP elevation were required for rescue
- Chronic dosing of HD models from pre-symptomatic ages confers additional benefit

Authors

Vahri Beaumont, Sheng Zhong, Hai Lin, ..., Christopher J. Schmidt, Margaret M. Zaleska, Ignacio Munoz-Sanjuan

Correspondence

vahri.beaumont@chdifoundation.org

In Brief

Beaumont et al. demonstrate that acute PDE10 inhibition boosts diminished corticostriatal input and indirect pathway output in symptomatic HD models, despite loss of PDE10. Their data provide rationale for a PDE10i clinical trial to assess symptom improvement in HD patients.

Accession Numbers

GSE89505
PXD005138

Beaumont et al., 2016, Neuron *92*, 1220–1237
December 21, 2016
http://dx.doi.org/10.1016/j.neuron.2016.10.064

CellPress

Neuron
Article

Phosphodiesterase 10A Inhibition Improves Cortico-Basal Ganglia Function in Huntington's Disease Models

Vahri Beaumont,[1,9,*] Sheng Zhong,[2] Hai Lin,[2] WenJin Xu,[2] Amyaouch Bradaia,[3] Esther Steidl,[3] Melanie Gleyzes,[3] Kristian Wadel,[3] Bruno Buisson,[3] Fernando E. Padovan-Neto,[4] Shreaya Chakroborty,[4] Karen M. Ward,[5] John F. Harms,[5] Jose Beltran,[2] Mei Kwan,[2] Afshin Ghavami,[2] Jenny Häggkvist,[6] Miklós Tóth,[6] Christer Halldin,[6] Andrea Varrone,[6] Christoph Schaab,[7] J. Nikolaj Dybowski,[7] Sarah Elschenbroich,[7] Kimmo Lehtimäki,[8] Taneli Heikkinen,[8] Larry Park,[1] James Rosinski,[1] Ladislav Mrzljak,[1] Daniel Lavery,[1] Anthony R. West,[4] Christopher J. Schmidt,[5] Margaret M. Zaleska,[5] and Ignacio Munoz-Sanjuan[1]

[1]CHDI Management/CHDI Foundation, 6080 Center Drive, Los Angeles, CA 90045, USA
[2]Psychogenics Inc., 100 Philips Parkway, Montvale, NJ 07645, USA
[3]Neuroservice, Domaine Saint Hilaire, CS30531, 595 rue Pierre BERTHIER, 13593 Aix-en-Provence Cedex 3, France
[4]Rosalind Franklin University of Medicine and Science, 3333 Green Bay Road, North Chicago, IL 60064, USA
[5]Neuroscience Research Unit, Pfizer, Inc., 610 Main Street, Cambridge, MA 02139, USA
[6]Department of Clinical Neuroscience, Karolinska Institutet, Centre for Psychiatry Research, R5:02, Karolinska University Hospital, 17176 Stockholm, Sweden
[7]Evotec (München) GmbH, Am Klopferspitz 19a, 82152 Martinsried, Germany
[8]Charles River Discovery, Microkatu 1, 70210 Kuopio, Finland
[9]Lead Contact
*Correspondence: vahri.beaumont@chdifoundation.org
http://dx.doi.org/10.1016/j.neuron.2016.10.064

SUMMARY

Huntington's disease (HD) symptoms are driven to a large extent by dysfunction of the basal ganglia circuitry. HD patients exhibit reduced striatal phoshodiesterase 10 (PDE10) levels. Using HD mouse models that exhibit reduced PDE10, we demonstrate the benefit of pharmacologic PDE10 inhibition to acutely correct basal ganglia circuitry deficits. PDE10 inhibition restored corticostriatal input and boosted cortically driven indirect pathway activity. Cyclic nucleotide signaling is impaired in HD models, and PDE10 loss may represent a homeostatic adaptation to maintain signaling. Elevation of both cAMP and cGMP by PDE10 inhibition was required for rescue. Phosphoproteomic profiling of striatum in response to PDE10 inhibition highlighted plausible neural substrates responsible for the improvement. Early chronic PDE10 inhibition in Q175 mice showed improvements beyond those seen with acute administration after symptom onset, including partial reversal of striatal deregulated transcripts and the prevention of the emergence of HD neurophysiological deficits.

INTRODUCTION

Huntington's disease is a neurodegenerative disease characterized by severe motor, psychiatric, and cognitive dysfunction (Biglan et al., 2013; Tabrizi et al., 2013), caused by an expansion of a polyglutamine-encoding CAG repeat in exon 1 of *huntingtin* (*HTT*) above 36 repeats (The Huntington's Disease Collaborative Research Group, 1993).

Degeneration of the caudate-putamen, progressive gray and white matter loss, whole brain, and regional atrophy (Tabrizi et al., 2013) has led to a focus on strategies to protect the brain from mutant (m)HTT-induced damage. With regard to circuitry dysfunction underlying HD symptoms, the cortico-striatal-thalamo-cortical circuit is particularly affected (Eidelberg and Surmeier, 2011). Neuropathologically, HD is characterized most clearly by a loss of GABAergic spiny projection neurons (SPNs) in the caudate-putamen. SPNs are innervated by glutamatergic neurons from the cerebral cortex and thalamic nuclei (Doig et al., 2010). In HD, this glutamatergic innervation is compromised, presumably resulting in less cortical control of basal ganglia function and SPN output (Unschuld et al., 2012).

SPNs are subdivided into two major classes. Indirect pathway (IP) SPNs (iSPNs) project densely to the external segment of the globus pallidus (GPe, GP in rodents). Direct pathway SPNs (dSPNs) project predominantly to the internal globus pallidus (GPi) and the substantia nigra pars reticulata (SNr). iSPNs and dSPNs play complementary roles in the control of movement and action selection: activation of iSPNs suppresses unwanted movements, whereas activation of dSPNs promotes cortical selection of particular actions (Nelson and Kreitzer, 2014). Chorea, a prominent symptom in adult-onset HD, is correlated with iSPN dysfunction. Postmortem evaluation of early-stage HD brains provides evidence for a preferential susceptibility of iSPNs to mHTT insult (Albin et al., 1992; Deng et al., 2004). The GPe also appears vulnerable, with cellular and volumetric loss equal to that of the caudate putamen (van den Bogaard et al., 2011).

In later stages of HD, this pathology also extends to dSPNs (Deng et al., 2004).

Early IP dysfunction provides a hypothesis to explain the hyperkinetic motor symptoms of (adult onset) HD patients: a reduction in iSPN output and disinhibition of GPe would lead to reduced subthalamic nucleus (STN) activity, diminished inhibition of motor thalamus, and impairment of motor control generated through aberrant motor cortex output. As the direct pathway (DP) becomes compromised later in disease pathology, a difficulty in initiating movements emerges, where characteristic bradykinesia and dystonic symptoms occur (Reedeker et al., 2010). In contrast, hypokinesic behaviors are the predominant feature of juvenile HD (JHD) (Letort and Gonzalez-Alegre, 2013), ascribed to "striatal failure", when both pathways (IP and DP) are affected. Interestingly, all HD pre-clinical rodent models carry CAG repeat expansions within or extending JHD CAG lengths (>50) and are predominantly hypokinetic (reviewed in Plotkin and Surmeier, 2015). Thus, HD rodent models may better represent JHD, displaying concurrent IP and DP dysfunction. Hence, it is challenging to robustly test drugs in HD models to predict any acute anti-choreic/anti-hyperkinetic potential in patients through evaluation of HD rodent behavior.

PDE10 belongs to a family of enzymes that hydrolyze cyclic AMP (cAMP) and cyclic guanosine monophosphate (cGMP). PDE10 is enriched in striatal SPNs where it regulates intracellular signaling and exerts a powerful control on striatal gene expression (Kleiman et al., 2011; Strick et al., 2010). PDE10 inhibition has been proposed to treat HD; the PDE10i TP-10 was reported to ameliorate motor and cognitive dysfunction and improved neuropathological abnormalities in the R6/2 HD mouse model when dosed from pre-symptomatic ages (Giampà et al., 2010; Giralt et al., 2013). Most interestingly, acutely, PDE10 inhibitors (PDE10i) are reported to enhance cortical responsivity of iSPNs, but not dSPNs in wild-type (WT) rats (Threlfell et al., 2009), which is reiterated directly by biochemical evidence showing greater induction of DARPP32 phosphorylation in response to PDE10i in iSPNs (~6-fold) versus dSPNs (~2-fold) (Nishi et al., 2008) and indirectly by behavioral consequences of PDE10i in rodents, where PDE10i mainly phenocopy D2 antagonists (putative activation of IP), suppressing rodent motor activity. Thus, PDE10 inhibitors may offer a unique way to acutely boost hypofunctioning IP activity in HD patients and combat especially hyperkinesic features of motor impairment.

Despite this, enthusiasm for this strategy was tempered by reports that PDE10 transcript and enzyme are dramatically reduced in HD patients, questioning whether further inhibition of PDE10 would be beneficial in a clinical context (Ahmad et al., 2014; Russell et al., 2014). Here, we extend observations on the benefit of a PDE10i for HD, focusing on the effects of acute PDE10 inhibition on restoration of the BG circuitry in HD models, particularly with the aim of assessing improvement in corticostriatal input and IP output deficits. Given the challenges of evaluating anti-hyperkinetic compounds behaviorally, we chose to look specifically at IP dysfunction in isolation in HD models, to provide a rationale for the acute use of PDE10i in correcting human HD hyperkinetic motor dysfunction.

RESULTS

PDE10i Elevates Cyclic Nucleotides in Symptomatic HD Models, Despite Dramatic Loss of PDE10 Enzyme

PET studies using novel PDE10 radioligands in HD patients have demonstrated an approximate 50% to 70% loss of PDE10 in the caudate putamen compared to controls (Ahmad et al., 2014; Russell et al., 2014). We first determined the extent to which HD models replicate this loss.

We undertook ex vivo radioligand binding studies with the PDE10-selective radioligand [^{3}H]-PF-04831704 to determine PDE10 B_{max} in R6/2 and Q175 mice. In striatal tissue from R6/2 and WT littermates at 6 weeks (early symptomatic) to 15 weeks of age (close to R6/2 end stage), PDE10 B_{max} had declined to 36% ± 5% of WT levels at 6 weeks ($p < 0.01$) and to 15% ± 2% of WT levels at 15 weeks ($p < 0.001$; Figure 1A). In the slower progressing Q175 full-length KI model, at a pre-symptomatic age (1.5 months) there was, if anything, a modest upregulation of PDE10 levels (114% ± 12% of average WT levels in Q175 heterozygous [het] mice and 120% ± 5% of WT levels in Q175 homozygous [hom] mice [$p < 0.05$]). However, in 8- to 9-month-old symptomatic animals, Q175 striatal PDE10 B_{max} levels were 56% ± 4% (het) and 42% ± 3% (hom) of WT levels (both $p < 0.0001$). Q175 het levels appeared similar at 12 months to those at 8 months (55% ± 2% of average WT B_{max}), but Q175 hom mice showed a further reduction to 26% ± 2% of average WT B_{max} (Figure 1B; both $p < 0.0001$). PDE10 loss was additionally corroborated in live 6-month-old Q175 mice using microPET to evaluate PDE10 levels using the PDE10 PET ligand [18F]MNI-659 in vivo (Figures 1C and 1D). Striatal BP_{ND} was 52% lower in Q175 het compared with WT animals ($p < 0.01$), slightly larger than the extent of reduction (40%) in D2 receptor levels assessed by [^{11}C]raclopride binding compared to WT at the same age ($p < 0.001$).

The age-dependent loss of striatal PDE10 levels in both Q175 and R6/2 mice was also seen by qPCR (Figure S1), demonstrating that reduced PDE10 levels is the consequence of transcriptional repression.

We investigated the impact of loss of PDE10 on ability of the selective PDE10i PF-02545920 (PF-920) to elicit functional responses in HD models (Figures 1E–1H). We measured cGMP changes using an ELISA, and cAMP changes were assessed using the phosphorylation status of CREB.

In 7- to 8-week-old R6/2 mice, subcutaneous (SC) injection of 1–10 mg/kg PF-920 elicited robust elevations in striatal cGMP and enhanced phosphorylation of CREB. The cGMP and pCREB response was modestly attenuated in R6/2 mice at 1 mg/kg. This corresponds to an expected occupancy of ~25%. This attenuation of effect in the HD models was alleviated at higher exposures (Figures 1E and 1F), and despite the fact that enzyme levels had declined by ~70%–80% at this age (Figure 1A), only the pCREB response was modestly attenuated compared to WT at the highest dose.

Evaluation of striatal cGMP elevation and CREB phosphorylation was performed in R6/2 and Q175 mice at different ages in response to 1 mg/kg SC PF-920. In HD models, the response to PF-920 declined as expected due to reduced enzyme levels, but was still readily observed at PDE10 levels >15% of WT B_{max}.

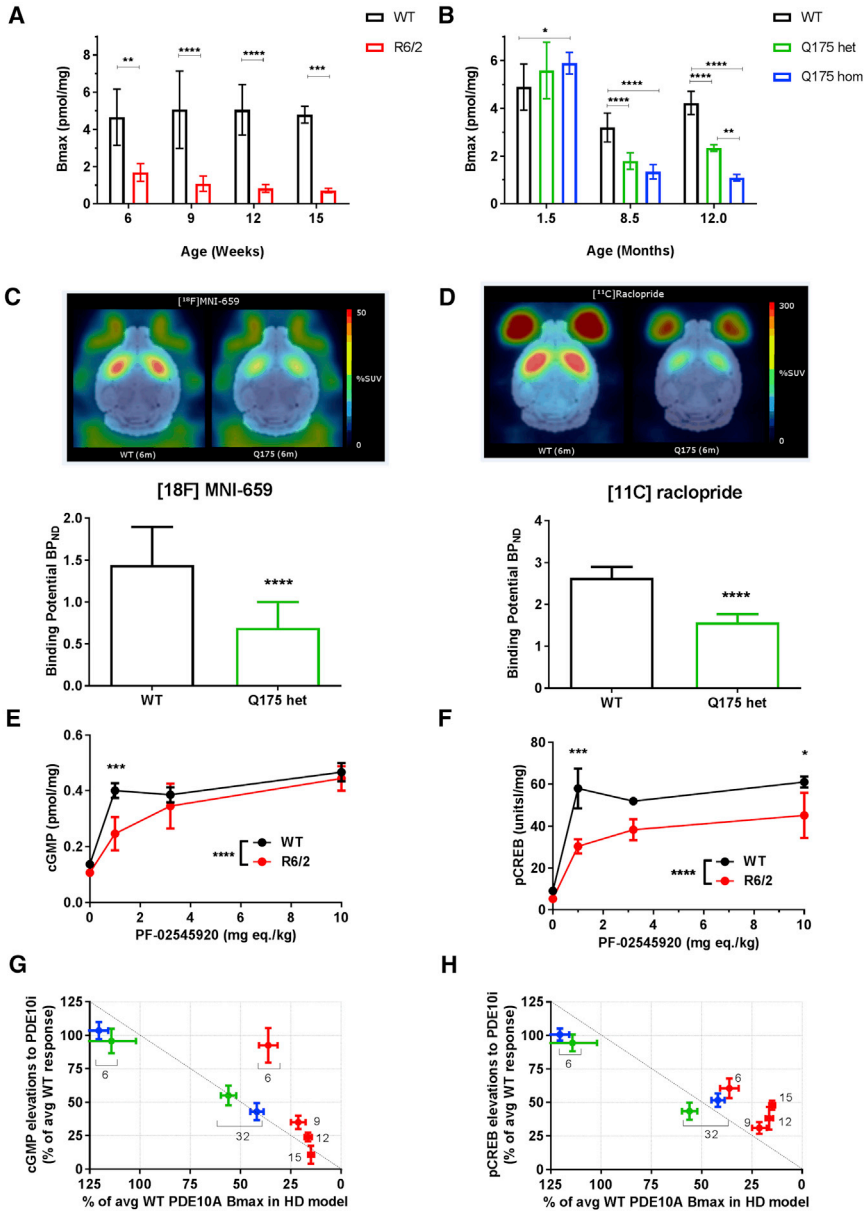

Figure 1. PDE10i Elevates Cyclic Nucleotides in HD Models, Despite Loss of PDE10

(A and B) Mean ± SD. PDE10 striatal B_{max} values in R6/2 (A) and Q175 mice (B) compared to aged matched WT (n = 4–8 per group).

(C and D) Mean PET images and mean ± SD BP_{ND} values of [^{18}F]MNI-659 (PDE10; C) and [^{11}C]raclopride (Drd2; D) in 6 month WT (n = 14) and Q175 mice (n = 15).

(E and F) Mean ± SEM striatal cGMP (E) or pCREB elevation (F) following acute SC PF-920 in 7–8 week R6/2 and WT (n = 5 per group).

(G and H) Percent ± SEM cGMP (G) and pCREB (H) increase in response to 1 mg/kg SC PF-920 plotted as % ± SD average WT response versus PDE10 loss relative to WT. red = R6/2, green = Q175 het, blue = Q175 hom (ages are shown as weeks). Dashed line indicates unity; the values above the line indicate greater response to drug than predicted by extent of enzyme loss.

The diminished response in Q175 mice to PDE10i correlated with the extent of enzyme loss. In R6/2 mice, there was a tendency for the pharmacodynamic response to be more robust than expected given the extent of enzyme loss (Figures 1G and 1H).

Rescue of SPN Neurophysiological Deficits following Acute PDE10 Inhibition in Symptomatic HD Models

We evaluated in vitro the effect of PDE10i on HD neurophysiological deficits using acute brain slices prepared from R6/2 and Q175 mice. We used 8-week-old R6/2 mice and 8- to 9-month-old Q175 het mice and the PDE10i PF-04898798 (PF-798). This compound has a K_d of 0.8 nM against rat PDE10A, and >1,000-fold selectivity over other PDEs.

SPNs in symptomatic R6/2 and Q175 mice display increased somatic membrane resistance (Rm), a depolarized resting membrane potential (Vm), and increased excitability in response to direct current injection (reduced rheobase), compared to SPNs recorded from age-matched WT (Heikkinen et al., 2012). Thus, HD SPNs are somatically hyper-excitable relative to WT SPNs, an observation corroborated by in vivo recordings where increased spontaneous firing activity has been noted in both the R6/2 and KI HD models (Miller et al., 2008, 2011). HD mice also display progressive impairment in responsiveness to cortical stimulation (Heikkinen et al., 2012; Miller et al., 2011). In combination, the loss of effective cortical innervation of the striatum, coupled with abnormal somatic excitability of SPNs within the HD striatum, would disrupt appropriate striatal information processing and resultant BG output.

80 nM PF-798 acutely reversed the hyper-excitability phenotypes of both R6/2 and Q175 SPNs. Vm, Rm, and rheobase were measured both prior to and 30 min following application of PF-798. PF-798 resulted in near total restoration of Vm and reversal of elevated Rm in HD model SPNs (Figure 2A), with no effect on WT SPN Vm and Rm. Thus, deficits in cyclic nucleotide signaling may underlie the aberrant resting state of HD SPNs. In contrast, PF-798 modestly increased rheobase of both WT and HD SPNs, but significant effects on this parameter were only noted in WT SPNs.

We assessed corticostriatal transmission by recording evoked excitatory post-synaptic currents (eEPSCs) upon stimulation of cortical afferents. Maximum eEPSC amplitudes were not different in either HD model as compared to WT (1,042 ± 166 pA versus 1,137 ± 168 pA for WT and R6/2, respectively, [n = 10 each], and 892 ± 89 pA versus 974 ± 143 pA for WT and Q175, respectively [n = 11 each]). However, slices from

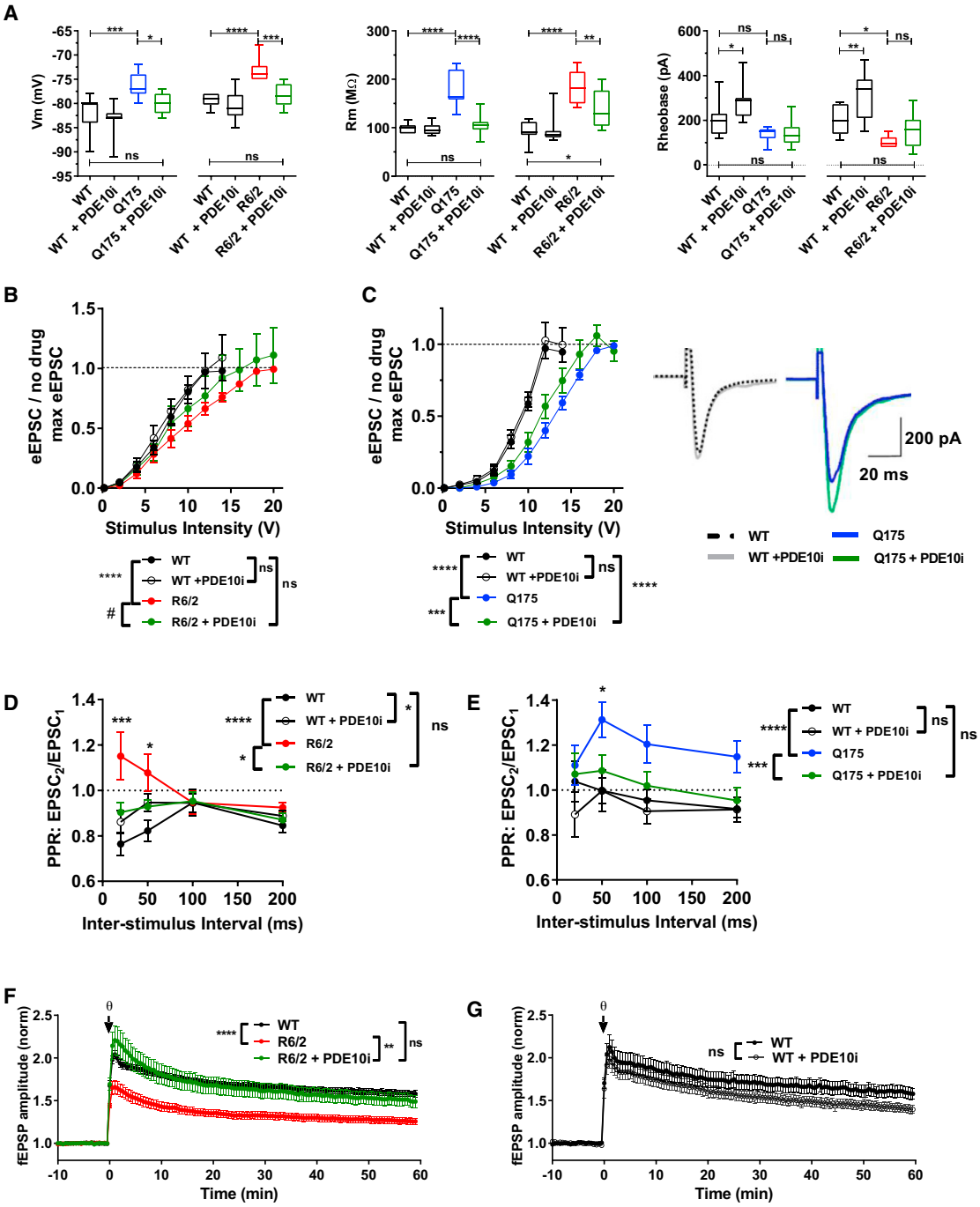

Figure 2. Rescue of SPN Neurophysiological Deficits and Hippocampal LTP in HD Models following Acute PDE10i

(A) SPN Vm, Rm, and rheobase from 8–9 month Q175 het and WT, and 7–8 week R6/2 and WT, pre- and post-PF-798 (80 nM). Data shown as box and whisker plots: box represents median and interquartile range, whiskers indicate minimum to maximum values.

(B and C) Corticostriatal eEPSC deficits in R6/2 (B) and Q175 het (C) are indicated by a rightward shift of I-O. PF-798 modestly increased transmission in HD slices at submaximal SIs.

(C) (Inset) Traces of EPSCs from a WT recording (SI 8 V) and Q175 het (SI 16 V) ± 80 nM PF-798. The traces average 20 recordings.

(D and E) PPR of eEPSCs. Both R6/2 (D) and Q175 het (E) show elevated PPR at shorter ISIs. The PF-798 (80 nM) restored HD PPR to WT levels.

(F and G) Hippocampal LTP is impaired in R6/2 and is restored to WT levels by PF-798 (80 nM) (F), WT LTP was unaffected (G).

(A–E) n = 10–11 per group.

(B–G) Mean ± SEM is plotted.

(F and G) n = 10–15 slices per group (minimum four animals per group).

symptomatic R6/2 and Q175 het mice required stronger stimulation intensity (SI) to elicit equivalent sized eEPSCs as those recorded from WT slices, resulting in rightward shifts of the input-output (I-O) characteristics (Figure 2B; WT versus R6/2; $p < 0.0001$) and (Figure 2C; WT versus Q175; $p < 0.0001$).

Acutely, PF-798 showed no significant effects on corticostriatal I-O characteristics in WT slices taken from either the R6/2 littermates (WT-R; Figure 2B) or Q175 littermates (WT-Q; Figure 2C) measured before and following application of the PDE10i. WT maximum eEPSCs before and after PDE10i treatment were also unchanged (1,042 ± 166 pA before and 1,015 ± 206 pA after PDE10i in WT-R slices [n = 10] and 892 ± 89 pA before and 912 ± 118 pA after PDE10i in WT-Q slices [n = 11]).

In R6/2 slices, there was no significant increase in eEPSC size in response to varying submaximal SIs after application of the PDE10i (Figure 2B; $p = 0.06$). Maximum achievable eEPSC size was unchanged (1,137 ± 168 pA prior to and 1,087 ± 163 pA post-PDE10i; n = 10). In Q175 het slices (Figure 2C), the enhancement of corticostriatal transmission at submaximal SIs after PDE10i was modest, but significant ($p < 0.0001$), with maximum achievable eEPSC size unchanged (974 ± 143 pA prior to and 1,024 ± 172 pA post-PDE10i; n = 11).

Employing a paired pulse paradigm with variable inter-stimulus intervals (ISI, 20 ms–200 ms; Figures 2D and 2E) revealed a reduction in EPSC paired pulse ratio (PPR) at shorter ISI following PF-798 treatment in R6/2, but not WT slices (Figure 2D), decreasing PPR to WT levels. PPR was also decreased in Q175 het slices at short ISI following PDE10i (Figure 2E).

This data indicate a modest acute improvement in corticostriatal transmission in HD slices after acute PDE10i treatment; representing only a small reversal of the HD deficits noted in this regard in vitro. No such effect was detected in WT slices.

In addition to striatal deficits, symptomatic R6/2 mice show deficits in hippocampal CA3-CA1 long-term potentiation (LTP) (Beaumont et al., 2014). PDE10 levels in hippocampus are low, but detectable (Giralt et al., 2013). PF-798 resulted in restoration of R6/2 LTP ($p < 0.01$, measured 20–60 min post-TBS; Figure 2F). The restoration of LTP was selective to R6/2 slices; the same application of PF-798 to WT slices had no effect on LTP (Figure 2G).

We asked whether restoration of R6/2 SPN Rm, Vm, and hippocampal LTP by PDE10i were mediated through elevation of cAMP or cGMP. Application of 8-Br-cGMP or a PDE9i, PF-4449613, which elevates only cGMP, partially or fully restored LTP deficits (Figures S2A and S2B; $p = 0.07$ and $p < 0.05$, respectively). Elevated HD SPN Rm was significantly restored ($p < 0.001$ and $p < 0.05$, respectively; Figure S2E). Conversely, elevations of cAMP alone, afforded either by acute application of 8-Br-cAMP or by inhibition of the cAMP-hydrolyzing PDE4 by rolipram, failed to affect R6/2 LTP deficits (Figures S2C and S2D). However, rolipram and 8-Br-cAMP did restore HD SPN Rm, as was seen with cGMP elevation ($p < 0.001$; Figure S2F). Together, these data do not unambiguously identify elevation in either cyclic nucleotide as solely responsible for the striatal improvement noted, but are in agreement that increased cGMP signaling is necessary and sufficient to restore hippocampal deficits in HD models (Nagy et al., 2015; Saavedra et al., 2013) and provides evidence that cGMP elevation contributes to the restoration of striatal deficits.

SPN Responsiveness to Cortical Stimulation In Vivo in Symptomatic Q175 Mice

We next assessed PDE10 inhibition in vivo on the responsiveness of SPNs and STN activity to cortical stimulation. In anesthetized 6- to 8-month-old Q175 het and WT mice, stimulation of M1 cortex resulted in SPN firing detected by extracellular single unit recordings in the striatum (Figure 3). In agreement with our in vitro slice data showing impaired corticostriatal transmission, Q175 het mice showed a decrease in the average number of stimulus-induced spikes that could be elicited (Figure 3C; $p < 0.01$). At higher SIs (1–1.4 mA), Q175 SPNs tended to respond to stimulation with single spike responses (65% of all responses) rather than multi-spike events (35%). This tendency was reversed in WT SPNs (66% exhibit multi-spike events versus 34% single spike responses; Figure 3B; $p < 0.05$). Q175 het mice also exhibited reduced spike probability in response to cortical stimulation ($p < 0.0001$; Figure 3D). Latency to spike firing was equivalent in both WT and Q175 mice (Figure 3E). There was no sex difference either in response within a genotype or in the extent of the Q175 het deficit relative to WT responses (i.e., both male Q175 [n = 21] versus WT [n = 16] response difference and female Q175 [n = 11] versus WT [n = 13] response difference = $p < 0.0001$; Table S8).

In the absence of stimulation, most WT SPNs (79%) were quiescent, and those that did show spontaneous activity (21%) did so infrequently (average firing rate [FR] of 0.07 ± 0.02 Hz [n = 5]). However, approximately double the number of Q175 SPNs showed spontaneous activity (48% of total; Figure 3F; $p = 0.08$), consistent with the lower rheobase and higher resting somatic membrane resistance recorded in vitro (Figure 2). The FR of those SPNs identified as "active" were also higher (Figure 3F; average FR 1.74 ± 0.8 Hz; $p < 0.05$) and showed higher intra-genotype variability than WT SPNs (F-test; $p < 0.0001$).

Enhancement of SPN Responsiveness to Cortical Stimulation following PF-02545920 Administration

To evaluate PDE10i, baseline I-O responses were obtained from SPNs recorded in a separate cohort of male WT (n = 10; Figures 3G and 3H) or Q175 het mice (n = 10; Figures 3J and 3K), prior to acute PF-920 (3.2 mg/kg sc) and following subsequent retest 30 min post-dose.

PF-920 enhanced evoked single unit activity in both WT and Q175 mice, as measured by an increase in spike probability (Figures 3G; $p < 0.001$ and 3J; $p < 0.001$) and an increase in the average number of spikes per stimulus (Figures 3H; $p < 0.001$ and 3K; $p < 0.001$). The enhancement in Q175 with PDE10i was sufficient to restore cortical responsivity to the level of WT vehicle-treated mice (Figure S3). The latency to first spike was unaltered in Q175 SPNs following PF-920 (data not shown; $p > 0.05$, two-way ANOVA), while PF-920 induced a significant decrease in onset latency in WT SPNs (data not shown; $p < 0.05$, two-way ANOVA). The finding that PDE10 inhibition also resulted in robust enhancement of WT SPN cortical responsivity in vivo is not surprising given previous publications (Padovan-Neto et al., 2015; Threlfell et al., 2009), although it differs from our results in the

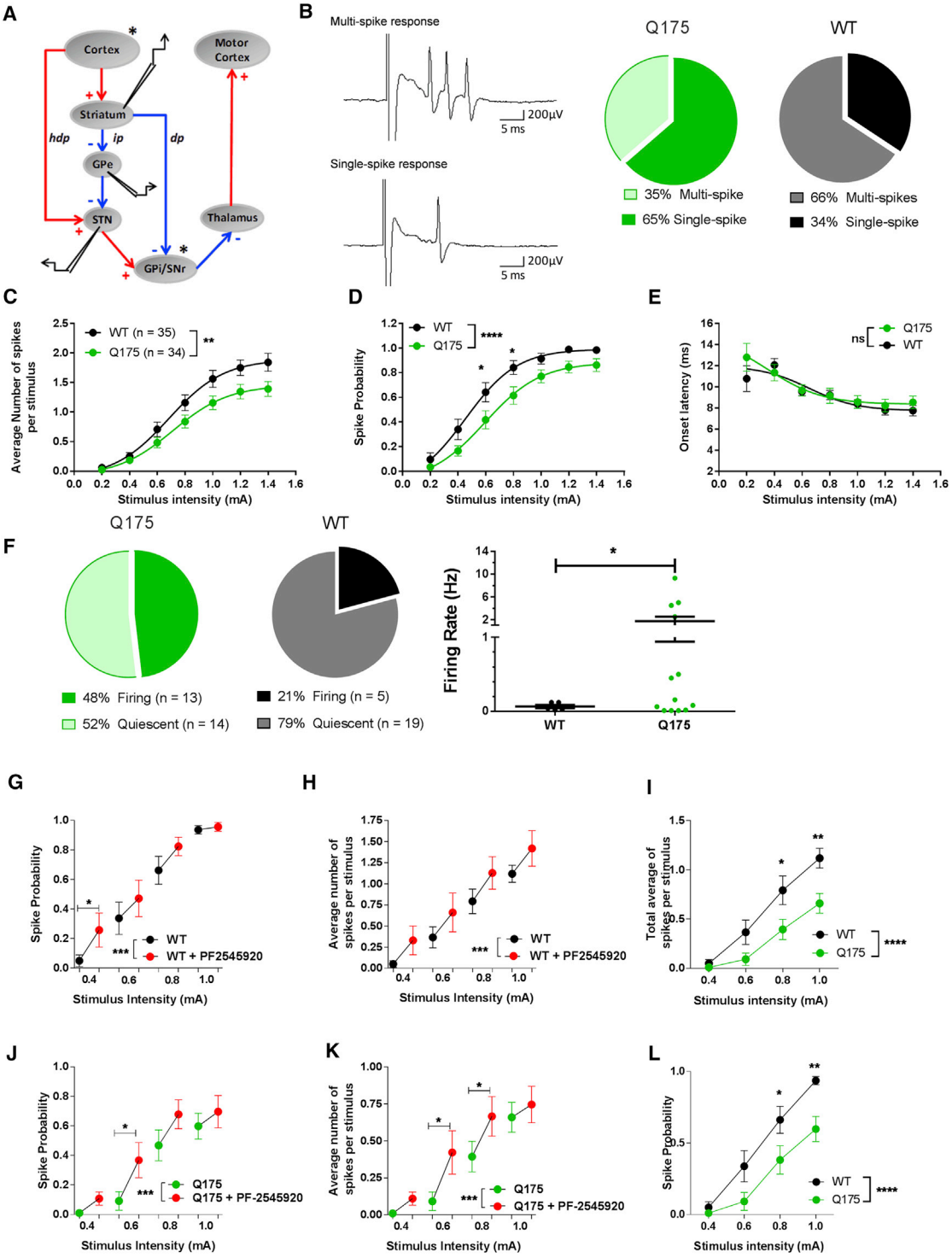

Figure 3. Corticostriatal Transmission Is Enhanced In Vivo by PDE10i

(A) Schematic of cortico-striatal, DP, IP, and HP pathways. In vivo stimulation (*) and recording sites are indicated. Red, glutamatergic; blue, GABAergic projection.

(B) Traces of SPNs responding to maximal stimulation of M1 cortex with a single spike or multiple spikes. Percent of response in Q175 het versus WT is shown.

(C and D) Average action potential number (C) and spike probability (D) in WT and Q175 het across a range of SIs.

(E) Latency of time to first action potential in WT and Q175 het.

(legend continued on next page)

in vitro slice preparation (Figures 2B and 2C). The reasons for this disconnect are unclear, but likely represent the modulation of a more complex network in vivo than is present in the slice preparation, where in the former case, all signaling pathways leading to modulation of cAMP and cGMP are intact.

Analysis of basal SPN activity recorded prior to and following PF-920 across WT and Q175 indicated no significant change in spontaneous FR or the proportion of spontaneously firing SPNs recorded in WT or Q175 mice pre- versus post-drug (Figure S3). Inter-spike interval or CV of inter-spike interval of striatal SPNs were unaffected (data not shown).

Enhancement of Indirect Pathway Activity following PF-02545920 in Symptomatic Q175 Het Mice

IP deficits in HD originating from decreased cortical activation of iSPNs may have consequences on the activity of downstream nuclei innervated by this projection or other deficits within the IP in HD models may account for IP hypo-activity. Thus, we monitored spontaneous GP and STN activity in a separate group of 6- to 8-month-old Q175 mice in vivo under anesthesia, followed by an evaluation of STN responsiveness to cortical stimulation in vivo.

Spontaneous GP Activity in WT, Q175 Het, and Q175 Hom Mice

Single unit extracellular recordings from the GP of WT, Q175 het, and Q175 hom were evaluated. There were three distinct firing patterns of units (regular, irregular, and burst firing) that were characterized by autocorrelograms. The majority of GP cells fired with regular and irregular patterns, while burst firing neurons represented <10% of all identified neurons. There was no change in firing pattern type preference between any genotype (Table S1).

Only modest alterations in GP spontaneous firing were seen in Q175 mice (Figures 4A and 4B). There was no significant change in FR (Table S1) or inter-spike interval variability (CV; $p = 0.12$; Figure 4C) for either regular or irregular firing units in Q175 het compared to WT mice. In Q175 hom, FR was unaltered compared to WT when all recordings were considered (Figure 4A). However, if parsed to regular or irregular firing units, neurons with regular firing patterns had enhanced FR (Figure 4B; Table S1; $p < 0.05$). CV was modestly enhanced ($p < 0.05$; Figures 4C and 4D); this was most apparent in regular firing pattern units ($p < 0.0001$; Figure 4D; Table S1). In addition, a small subset of cells in Q175 hom showed abnormally prolonged silent gaps between firing (silent periods lasting >5% of the total recording time; i.e., >20 s for a 5 min recording session). There were six units (of 113 regular/irregular firing neurons recorded) that were identified: this type of activity was never seen in Q175 het or WT mice (data not shown).

Decreased Spontaneous STN Activity in Q175 Mice

Single unit extracellular recordings from the STN revealed irregular and burst firing units, with negligible regular firing units. There was no obvious change in firing pattern type preference between WT and Q175 hom, but we recorded significantly more neurons categorized as "burst firing" rather than "irregularly firing" in Q175 het mice compared to WT ($p < 0.05$; Table S2). Overall, FR of STN neurons in both Q175 het and hom mice were reduced compared to WT littermates when averaged FR of burst and irregular neurons were combined ($p < 0.05$ and $p < 0.01$, respectively; Figures 4E and 4F). This was driven by a modest reduction of FR in irregular firing neurons in Q175 hom, but most largely through a substantial increase in inter-burst interval in "bursting" units in both Q175 het ($p < 0.0001$) and hom ($p < 0.001$); (Table S2). We also encountered a higher number of potentially "silent units" in Q175 hom mice, as defined by the reduced probability of finding active units per attempt relative to WT (Figure 4G; recording success rate: WT, 33/42 = 0.79; Q175 het, 23/29 = 0.79 (ns compared to WT); Q175 hom, 13/25 = 0.52; and $p < 0.0001$ compared to WT).

Reduced Cortico-STN Responsiveness in Q175 Het Mice

The cortical responsiveness of the STN to M1 stimulation was subsequently examined in 6- to 8-month-old mice. In addition to being under cortical control through the polysynaptic IP, the STN receives a direct excitatory input from the cortex (the hyperdirect pathway, or HP; Figure 3A). Concordant with this, a substantial number of STN neurons respond to cortical stimulation with a clear biphasic excitatory response (Figure 4H), and we concentrated exclusively on recordings that showed this pattern of innervation. We speculated that the first short latency phase likely represents the HP monosynaptic innervation of STN (latency 2–15 ms), with the longer latency second excitatory phase (latency 16–50 ms) driven by the polysynaptic IP projection (Kolomiets et al., 2001).

A comparison of WT and Q175 het I-O curves showed that in Q175, both the responsiveness of the STN Phase 1 and 2 components were significantly attenuated (Figure 4I). In this response, Q175 het males appeared solely to contribute to the impairment at the age we studied (Figure S4).

PF-02545920 Increased Indirect Pathway Activity and Modulated STN Firing Rate

To establish the PDE10i effect on cortically driven STN firing, we delivered PF-920 via intravenous (i.v.) bolus injection through a jugular vein catheter, after first establishing the stability of Phase 1/2 STN recordings to two subsequently delivered 1 mL/kg vehicle injections spaced 20–25 min apart (Figures S4C and S4D). PF-920 (1.5 mg/kg) was subsequently compared against a vehicle baseline response obtained 20–25 min prior to compound injection (Figure 5). In 6- to 7-month-old WT ($n = 6$) and Q175 het ($n = 7$) mice, PF-920 resulted in enhancement of only the Phase 2 evoked single unit activity (Figures 5C and 5D; WT $p < 0.0001$ and Q175 $p < 0.0001$), indicating selective activation of the cortically driven IP, but not putative HP (Phase 1) pathway (Figures 5A and 5B). The "Phase 2" enhancement was of equal magnitude in both Q175 het and WT mice. The enhancement

(F) Percent and average FR of spontaneously active SPNs in Q175 het versus WT.
(G–L) PF-920 (3.2 mg/kg sc) enhanced spike probability and the average number of spikes per SI in both WT (G and H) and Q175 (J and K) mice ($n = 10$ each). The pre-drug genotype effects were confirmed in these separate cohorts of mice, despite lower sample sizes than in (C) and (D) (I and L).
(C–L) Mean ± SEM is plotted.

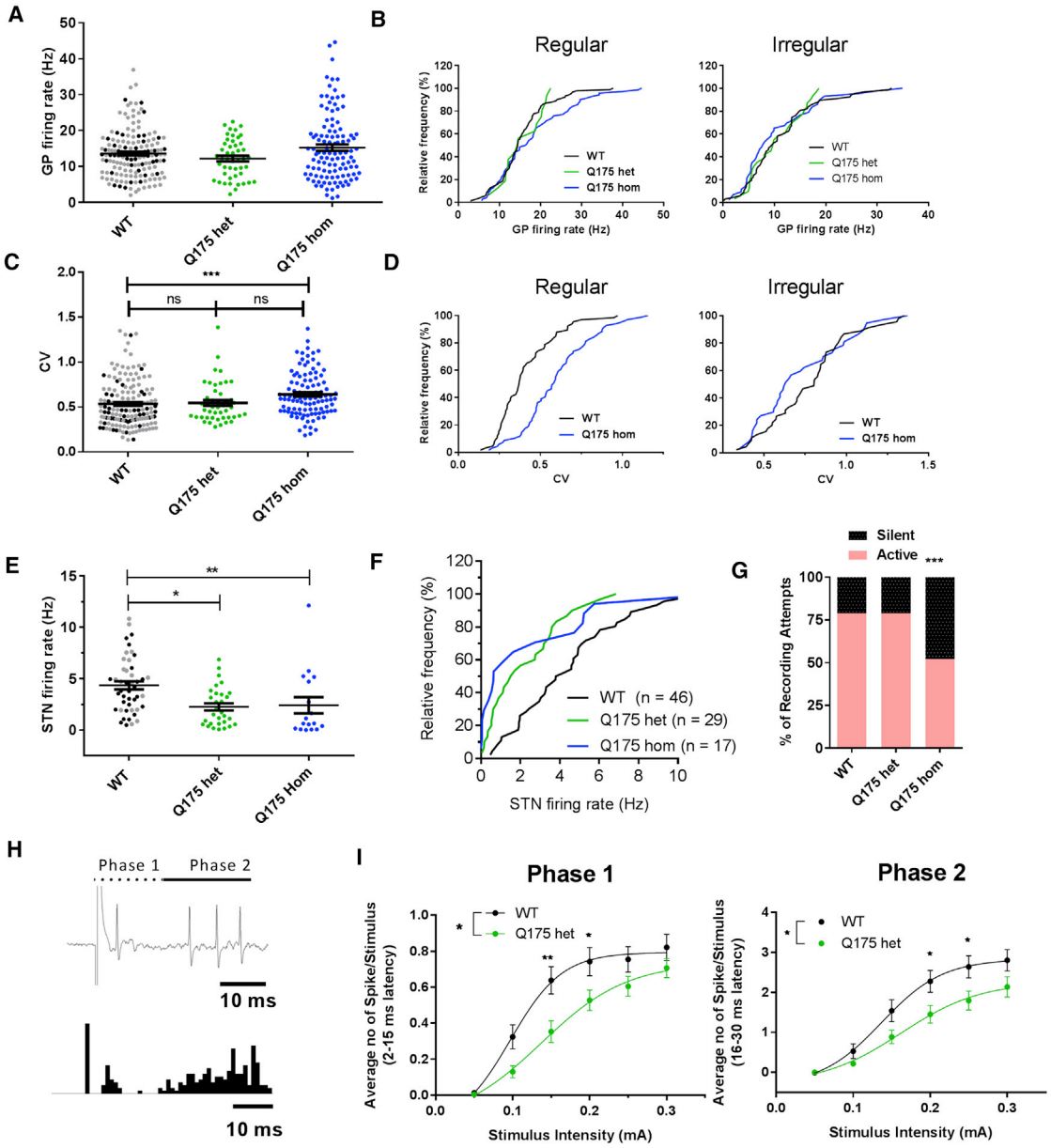

Figure 4. GP and STN Firing Rate Properties and Cortico-STN Transmission in Q175 Mice Are Altered

(A–D) GP neuron firing properties.

(A) Spontaneous single unit GP FR in WT, Q175 het, and hom mice. The plot shows combined rates from irregular and regular firing GP neurons. WT combined from WT to het group (closed circles) and WT to hom group (open circles) are shown.

(B) Relative frequency of regular and irregular GP FR in WT, Q175 het, and hom mice.

(C) Increased GP CV in Q175 hom mice.

(D) Relative frequency of regular and irregular firing units CV score in WT versus Q175 hom mice. Increased CV in Q175 hom is attributed to regular firing neurons.

(E–G) STN neuron firing properties.

(E) Spontaneous STN FR is decreased in Q175 het and hom mice.

In (A), (C), and (E), mean ± SEM is shown.

(F) Relative frequency of STN FR in WT, Q175 het, and hom mice.

(G) % of recording attempts in WT and Q175 mice resulting in identification of active STN single units.

(H and I) Responsiveness of STN to M1 cortical stimulation.

(H) (Upper image) A typical STN neuron response to M1 stimulation occurs in two phases. The binned histogram plot of responses to 50 repeated stimuli separate the two response phases is shown (lower).

(I) Cortico-STN I-O response of WT and Q175 het mice separated according to Phase 1 (HP) or Phase 2 (IP) response. Mean ± SEM is plotted.

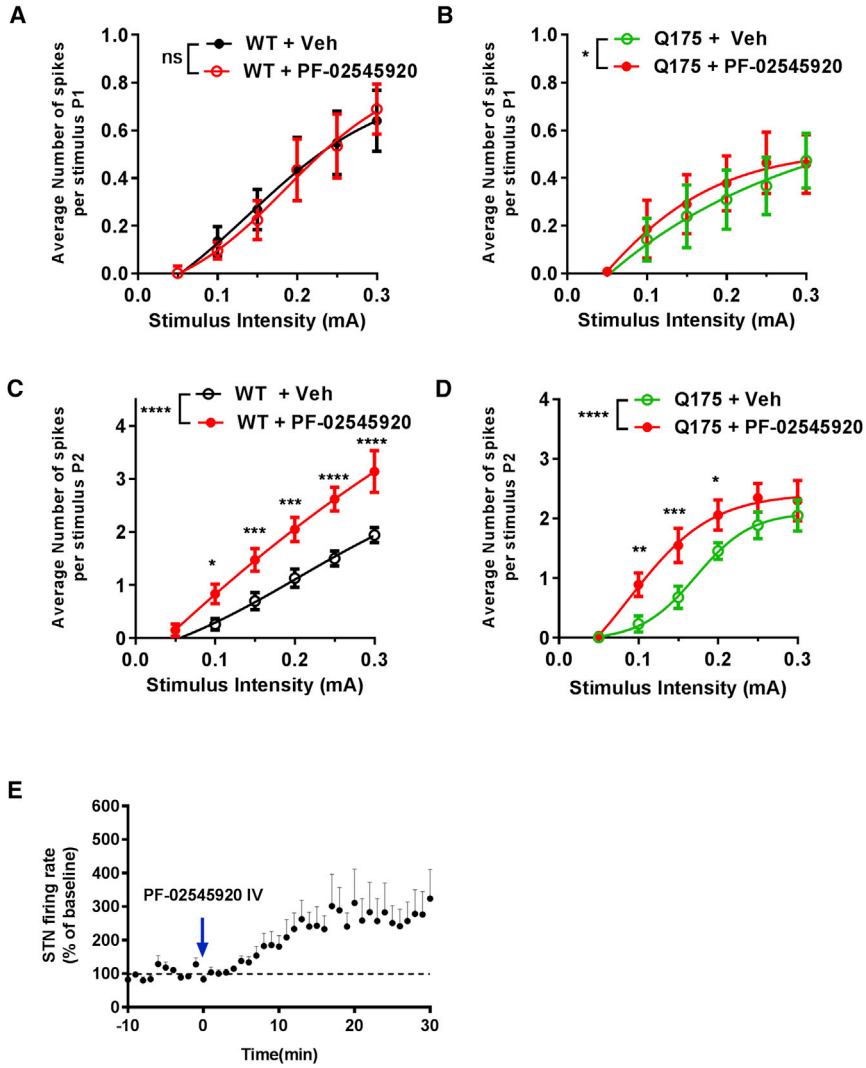

Figure 5. Cortico-STN Transmission In Vivo Is Enhanced by Acute PDE10i

(A and B) Phase 1 (HP) cortico-STN transmission is unaltered following acute PDE10i i.v. in WT (A) and modestly enhanced in Q175 (B).

(C and D) Conversely, Phase 2 (IP) cortico-STN transmission is enhanced following PDE10i i.v. in WT (C) and Q175 het (D). WT, n = 6 and Q175 het, n = 7.

(E) STN spontaneous FR in response to PDE10i i.v. was recorded in a subset of mice (n = 2 Q175 and n = 3 WT mice; data combined). (Note, in A–D, between genotype comparisons should not be made due to low statistical power for this comparison; estimated at <0.35, see Figure S4A). Mean ± SEM is plotted.

of IP output in Q175 mice by PDE10i would thus serve to correct this hypo-functioning pathway. In a limited number of recordings, we also monitored spontaneous STN firing rate before and after the PDE10i was delivered i.v. (n = 2 Q175 and n = 3 WT; Figure 5E; data shown is pooled). STN FR was robustly enhanced by ~3-fold in both WT and Q175 het mice, as would be expected via IP activation.

Global Proteomic and Phosphoproteomic Analyses of WT and Q175 Mice Striata and Response to PF-02545920 Reveal Downstream Targets and Pathways Relevant to HD

To address how elevation of cAMP and cGMP are restorative in HD models, we evaluated the striatal phosphoproteome in 6-month-old WT (n = 10), Q175 het (n = 9), and hom (n = 9) mice in response to a single administration of 3.2 mg/kg PF-920 or vehicle for 1 hr. Mass spectrometry (MS)-based global and quantitative proteome and phosphoproteome analysis was applied to the striatal tissues to assess differential expression of proteins and their phosphorylation in response to PDE10i treatment (accession number PRIDE: PXD005138). Peptides were labeled with mTRAQ to allow precise comparison between vehicle and PDE10i treatment. At the same time, the MaxLFQ intensities were used for comparison across genotypes. In total 8,152 proteins and 18,928 phosphorylation sites were detected. Since not all proteins and phosphorylation sites were quantified in all samples, only the 5,076 proteins and the 10,506 phosphorylation sites that were quantified in more than two thirds of the samples were used for analysis.

Q175 Genotype Differences in the Striatal Proteome Implicate Cyclic Nucleotide Signaling Pathway Deregulation

Differences in striatal protein expression between WT, Q175 het, and Q175 hom were assessed by applying a one-way ANOVA to the label-free intensities of the vehicle-treated mice. There were 154 of the 5,076 proteins identified by MS that were found to have a significant difference in abundance between at least two genotypes. A rank ordered list is provided in Table S3. In agreement with the recognition that increasing CAG expansion inversely correlates with expression of HTT (Alexandrov et al., 2016), HTT was the most decreased protein identified in Q175 hom (~6-fold decrease), with a ~2-fold decrease in Q175 het. The HTT interactor HAP40 (F8a1) was the second most deregulated protein. Interestingly, HTT and huntingtin associated protein 1 (HAP1) levels were anti-correlated, HAP1 being the most upregulated protein identified in Q175 striatum. Enrichment analysis indicated mainly upregulation of terms associated with the ubiquitin proteasome system, protein translation, and metabolism (KEGG) and a downregulation of terms associated particularly with membrane channel activity (GO) (Table S3). Further curation indicated that many of these proteins had been identified as aberrantly expressed in other HD model systems, with 23 proteins (15%)

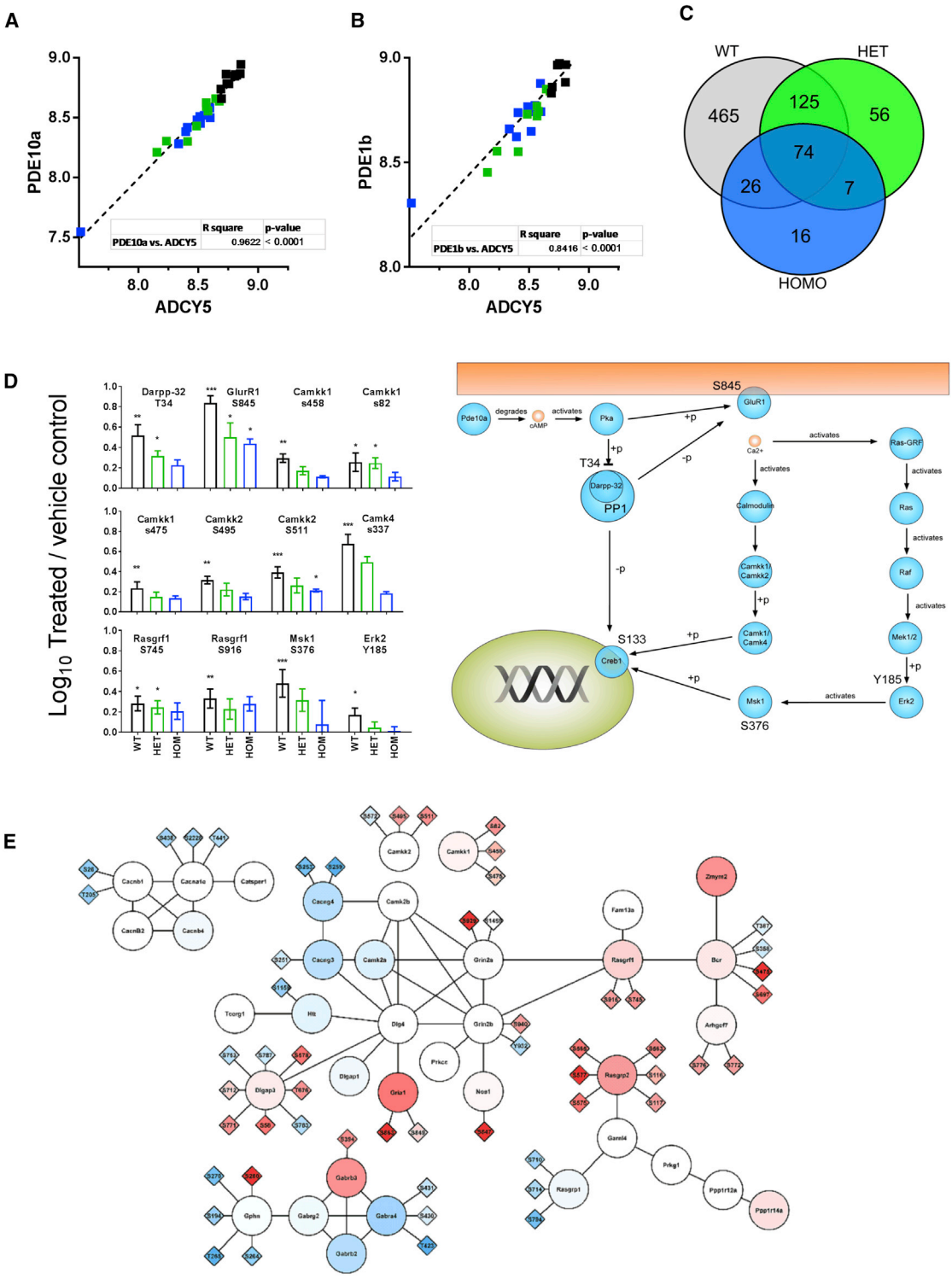

Figure 6. Homeostatic Regulation of Cyclic Nucleotide Signaling in HD Models

(A and B) Correlation of PDE10 (A) or PDE1b (B) to ADCY5 protein loss in 6 month Q175 het, hom, and WT striatum.

(C) Venn diagram showing overlap of significantly regulated ($p < 0.05$) phosphorylation sites.

(legend continued on next page)

previously identified as direct HTT interactors. Our analysis points to aberrant membrane receptor sorting and trafficking through the endosomal/lysosomal degradation pathways, alterations in axonal guidance, axonal transport, and cell adhesion signaling pathways that underlie dendritic and synaptic maintenance and plasticity, and DNA damage and repair pathways.

GO terms associated with cyclic nucleotide PDE activity were also identified ($p = 0.06$). Of the proteins involved in cyclic nucleotide processing, a strong decrease in adenylate cyclase type 5 (ADCY5) expression in Q175 mice was seen, as well as decreases in PDE10 and PDE1b enzyme. ADCY5 is the most highly expressed striatal adenylate cyclase (Matsuoka et al., 1997). ADCY5 loss was correlated with PDE10 ($R^2 = 0.96$, $p = 9.6 \times 10^{-21}$) and PDE1b loss ($R^2 = 0.84$, $p = 2.6 \times 10^{-12}$), suggesting tight homeostatic coupling maintaining equilibrium between cAMP production and degradation (Figures 6A and 6B). Thus, decreased expression of ADCY5 may compensate to reset cAMP levels due to decreased expression of PDE10 and PDE1b, or indeed, vice versa. In a study evaluating the time-dependent striatal proteomic signature of Q175 and Q20 het (control) KI mice at 2, 6, and 10 months, the correlation between ADCY5 and PDE10a levels was confirmed (Figure S5A). In contrast, a much weaker correlation between HTT expression and PDE10a or ADCY5 levels in the striatum of Q175 mice was seen (Figures S5B and S5C; Table S8).

The Basal Striatal Phosphoproteome Was Unaltered in Q175 Mice

Using the phosphosite intensities of vehicle-treated mice and following normalization of the phosphosite intensities by protein intensities, no significantly differentially regulated sites were identified between WT and Q175 mice.

PF-02545920-Induced Changes in the Phosphoproteome

Following acute PF-920 treatment, 690 significantly regulated phosphosites were identified in WT mice, 262 in Q175 het, and 123 in Q175 hom (Figure 6C; Table S4), from a total of 8,683 unique phosphorylation sites that were quantified in more than two thirds of the samples in WT, 9,190 in Q175 het, and 8,602 in Q175 hom.

PDE10 inhibition is known to increase phosphorylation of CREB-1 at Ser133, leading to its activation and triggering gene expression (Siuciak et al., 2006). While the tryptic peptide containing CREB-1 Ser133 is too short (~4 amino acids; PSYR) to be detected by our global phosphoproteome technology, we found a strong phosphoproteomic signature suggesting robust CREB activation in WT mice (Figure 6D). Glutamate receptor GRIA1 Ser863 (equivalent to Ser845 in humans) phosphorylation was enhanced in all genotypes, which enhances channel open probability to recruit CamK and microtubule-associated protein (MAP) kinase pathways to activation of CREB transcription (reviewed in Traynelis et al., 2010). Phosphosites on CaMKK1/2 and CaMK4 were found to be significantly regulated by PDE10i, supportive of engagement of the CamK4-mediated CREB-1 S133 phosphorylation (Figure 6D). MAP kinase pathway activation was also apparent: RAS guanylate nucleotide-releasing proteins (RASGRP1/2) and Ras-specific guanine nucleotide-releasing factor 1 (RASGRF1) were regulated at several sites, activating the RAS/RAF/MEK/ERK cascade, with resultant ERK2 Tyr185 and MSK1 Ser376 phosphorylation in WT mice upon treatment (Figure 6D). PPP1R1B (DARPP-32) Thr34 phosphorylation sites were also significantly upregulated upon treatment in all genotypes, except in Q175 hom ($q = 0.1$). This leads to a diminution of protein phosphatase 1 (PP1) activity resulting in enhanced CREB-1 phosphorylation and multiple downstream effectors (Nishi et al., 2008).

Despite the fact that phosphorylation was blunted in Q175 mice, particularly in the hom mice, where the same sites often did not meet the specified false discovery rate (FDR) criteria for significance ($p < 0.05$), CREB activation was apparent, if attenuated. Enrichment analysis revealed eight enriched GO terms in WT and het, and three in hom, all primarily relating to activation or regulation of transcriptional mechanisms (Table S4). In the case of KEGG enrichment analysis, MAP kinase signaling cascades in WT and het were noted (Table S4).

PF-920-induced phosphosite changes were mapped onto the STRING protein-protein interaction network. Using the SubExtractor Algorithm, which combines proteomic data with protein-protein interaction data via a Bayesian probabilistic model, additional regulated subnetworks were identified (Figure 6E for Q175 het; subnetworks for wild-type and Q175 hom are shown in the Figure S6).

This analysis identified phosphorylation changes in a variety of scaffolding and membrane proteins important for the regulation of synaptic transmission and neuronal excitability, mechanisms that may contribute more acutely to the restoration of membrane excitability in HD SPNs and the regulation of SPN responsiveness to cortical stimulation. These include changes seen in glutamate and GABAergic signaling compartments, AKAPs, GKAPs, as well as ion channel regulation that helps maintain membrane excitability (see Table S5 for details).

PF-02545920-Induced Changes in the Proteome

Proteomic changes induced by PF-920 were tested in each genotype separately using the one-sample Mean Rank test on mTRAQ log-ratios between PDE10i and vehicle control treated protein intensities. In total, 5,280, 5,426, and 5,379 proteins were quantified in more than two thirds of the samples in the WT, Q175 het, and hom mice, respectively. Unsurprisingly, given the acute dosing paradigm used, only one protein, the transcription factor jun-B (JUNB), was upregulated in all genotypes by more than 2-fold. JUNB is an immediate early gene (IEG) expressed following CREB activation (Herdegen and Leah, 1998),

(D) Mean Log10 ratio of PF-920/vehicle-treated phosphoproteome changes observed in signaling pathways resulting in activation of CREB (accompanying diagram in right panel). Mean ± SEM across replicates (* = $q < 0.05$, ** = $q < 0.01$, and *** = $q < 0.001$).

(E) The Q175 het protein subnetwork identified using the Subextractor algorithm. Spheres = proteins, colored according to the average regulation of all identified phosphosites. Diamonds represent phosphosites (red, upregulated; blue, downregulated).

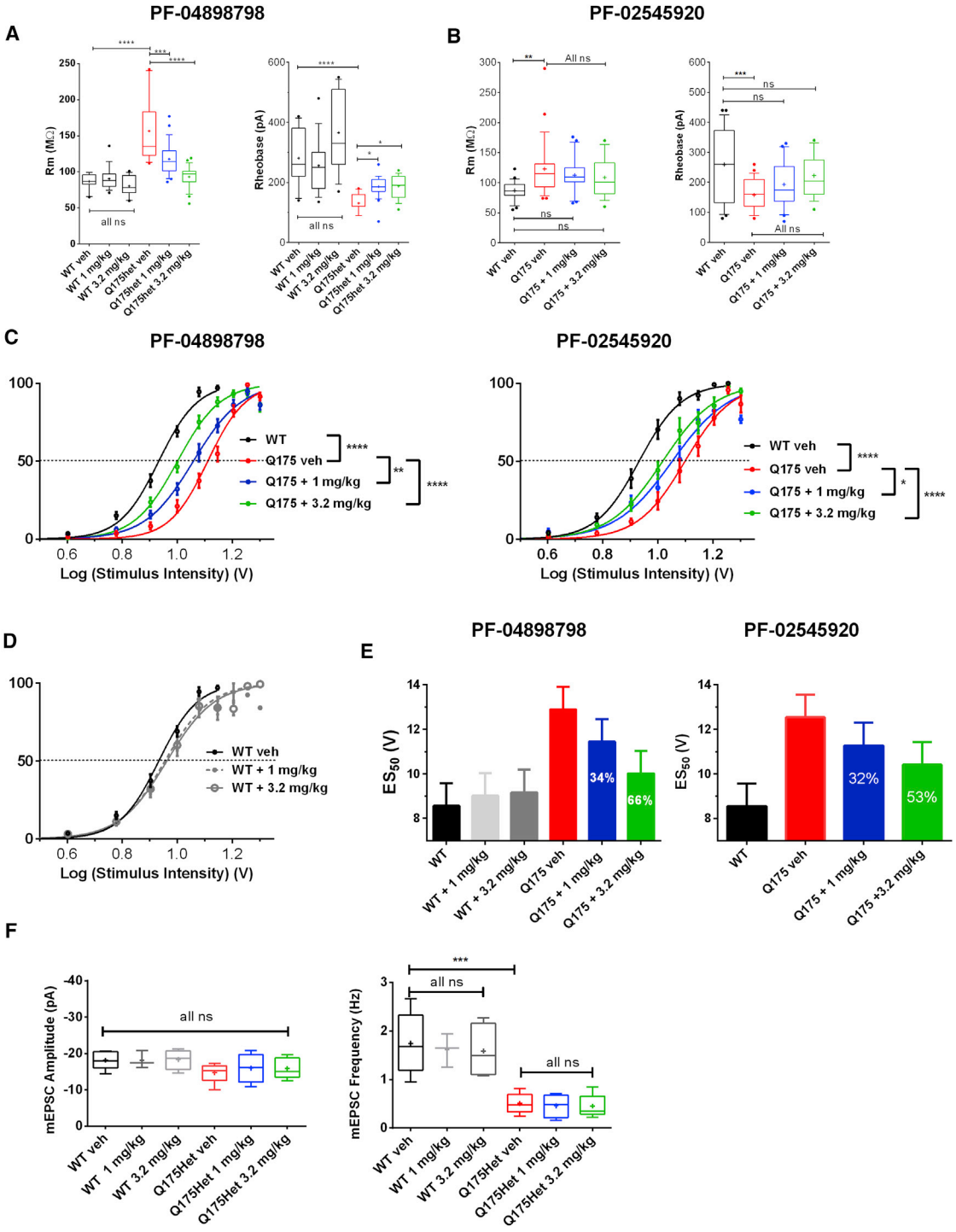

Figure 7. Chronic PDE10i Treatment Prevents Emergence of Neurophysiological Deficits in Q175 Het Mice

(A and B) SPN Rm and rheobase from 6- to 7-month-old Q175 and WT corticostriatal slices following a 4 month *po bid* dosing schedule with either vehicle or PF-798 (n = 11–24 per group, A) or vehicle and PF-920 (n = 18–28 per group, B). Data shown as box and whisker plots: the box represents median and interquartile range, + represents mean, whiskers indicate 10–90 percentile values, outliers are shown (dots).

(C) PF-798 (n = 11–23 per group) and PF-920 (n = 8–11 per group) partially and dose-dependently prevented emergence of corticostriatal deficits in Q175 hets.

(D) PF-798 (n = 13–15 per group) had no effect on WT corticostriatal transmission.

(legend continued on next page)

leading to support of significant CREB activation in PDE10i treated mice.

Prevention of SPN Hyperexcitability and Corticostriatal Transmission Deficits following Chronic PDE10i in Symptomatic Q175 Mice

Given the acute actions of PDE10i in partially restoring key HD-relevant circuit abnormalities in HD models, and the transcriptional role of the cGMP/PKG and cAMP/PKA/CREB signaling cascade in synaptic plasticity, we lastly assessed whether long-term dosing could delay the emergence of these phenotypes. Ex vivo slice recordings were made from 6-month-old Q175 het mice having undergone a 4-month dosing schedule with either of the PDE10i PF-798 or PF-920 at 1 and 3.2 mg/kg *po bid*; compared to both WT and Q175 het mice dosed with vehicle alone. Mice were sacrificed and recordings were made 3–14 days post-last dose. No compound was present during the recordings, meaning that any observed change in the parameters tested could be ascribed to an improvement on corticostriatal or SPN function that arose from the chronic dosing regimen, rather than acute drug action.

As before, the major genotypic differences noted between the vehicle-treated Q175 het and WT groups were increased SPN Rm, decreased rheobase (Figures 7A and 7B), and a right-shifted corticostriatal I-O curve (Figure 7C). Treatment with PF-798 showed a robust dose-dependent reversal of the Q175 SPN elevated Rm (1 mg/kg = $p < 0.001$ and 3.2 mg/kg = $p < 0.0001$), as well as modest improvement in rheobase ($p < 0.05$; Figure 7A). PF-798 dosed WT mice showed no effect on these parameters (Figure 7A). In PF-920 dosed Q175 het mice, we saw no effect on Q175 SPN Rm or rheobase compared to the vehicle-treated control group; however, Q175 drug-treated groups were not statistically significantly different from the WT vehicle group in this study (Figure 7B). A hint of improvement (ns by ANOVA with Tukey's post hoc test, $p < 0.01$ by unpaired t test) in rheobase was noted in the group of mice that received 3.2 mg/kg PF-920.

In both PF-798 and PF-920 treated Q175 mice, we saw dose-dependent improvement in corticostriatal transmission compared to the respective Q175 vehicle-treated control group (PF-798 at both 1 and 3 mg/kg = $p < 0.0001$; PF-920 at 1 mg/kg = $p < 0.05$; and at 3.2 mg/kg = $p < 0.0001$; Figure 7C). In WT mice dosed with PF-798, corticostriatal transmission was unaffected relative to the vehicle control (Figure 7D). An estimate of the maximal extent of rescue of corticostriatal transmission by PDE10i was given by measuring the effective SI required to achieve half maximal eEPSC response size (ES_{50}) per dose group (Figure 7E). Prolonged treatment of Q175 het mice with either 3.2 mg/kg PF-798 or 3.2 mg/kg PF-920 prevented the emergence of corticostriatal transmission deficits in Q175 het mice relative to WT by 53%–65%. This data provide evidence for a prevention of emerging corticostriatal and SPN dysfunction afforded by early, daily PDE10i administration in HD models. Surprisingly, a concomitant improvement in non-action potential dependent release through evaluation of mEPSCs in Q175 mice after PF-798 dosing was not seen (Figure 7F). While this may indicate that the enhancement of transmission by PDE10i did not arise directly from modulation of glutamatergic transmission per se, mEPSCs arise from spontaneous release from both thalamostriatal and corticostriatal terminals. Thalamostriatal synapses have higher release probability than corticostriatal synapses (Doig et al., 2010) and as such may contribute more to mEPSCs than corticostriatal synapses, explaining this disparity. Alternatively, spontaneous neurotransmission may operate independently of evoked transmission via distinct pre- and post-synaptic substrates (Kavalali et al., 2011), which are not impacted by PDE10i.

RNA-Sequencing Analyses Reveals a Robust Transcriptional Response to Chronic PDE10 Inhibition in Q175 and WT Mice

To address the impact of chronic PDE10i on the transcriptional dysregulation associated with HD progression, WT and Q175 hom mice were dosed from 5 weeks to 9 months of age with vehicle alone or PF-920 (0.32, 1.0, and 3.2 mg/kg *po qd*). Body weight and neurological index were measured; PDE10i was without effect on these parameters (Figure S7). Brain volume was monitored by repeated in vivo MRI scanning at 6 weeks, 4 months, and 8 months of age. Striatal, but not cortical or whole brain, volume was modestly, but significantly, improved in the 3.2 mg/kg PF-920 group. However, during this study, we determined that brain volume deficits in Q175 hom appeared prior to treatment start and were possibly developmental in nature, so the significance of this modest treatment effect is unclear (Figure S7). We also conducted limited motor evaluation using open field and rearing-climbing tests. Climbing behavior and distance traveled in the open field were modestly enhanced in mice treated with 3.2 mg/kg PF-920 (Figure S8).

At 9 months of age, on the last day of dosing, cortical and striatal tissues were harvested 1 hr post-last dose and deep RNA sequenced (GEO: GSE89505). Over 5,000 genes showed statistically significant genotype differences (Table S6; FDR-protected p value < 0.05). Overall, 669 striatal transcripts were differentially regulated following PF-920 treatment (Table S7). The PDE10i transcriptional signature was not associated with changes in the levels of Htt, ADCY5, or PDE10 mRNAs. Ingenuity pathway analysis revealed an involvement of cAMP-mediated signaling ($p = 1.1 \times 10^{-4}$) and G protein coupled receptor signaling ($p = 5.2 \times 10^{-4}$), as well as circadian and GADD45 signaling pathways. Predicted upstream regulators were CREB1 (Figure 8A; $p = 5.2 \times 10^{-28}$) and cAMP responsive element modulator (CREM; Figure 8D; $p = 3.2 \times 10^{-32}$). We also found evidence of modulation of MAPK/ERK signaling, as several dual-specificity phosphatases were upregulated,

(E) Estimate of PDE10i induced rescue of corticostriatal transmission from (C), plotted as ES_{50}. Mean ± SEM shown.
(F) mEPSC amplitude and frequency from PF-798 dosed mice (n = 5–9 per group). The improvement in corticostriatal transmission (C) was not mirrored by an improvement in non-action potential dependent glutamatergic transmission.
(C–F) Mean ± SEM is plotted.

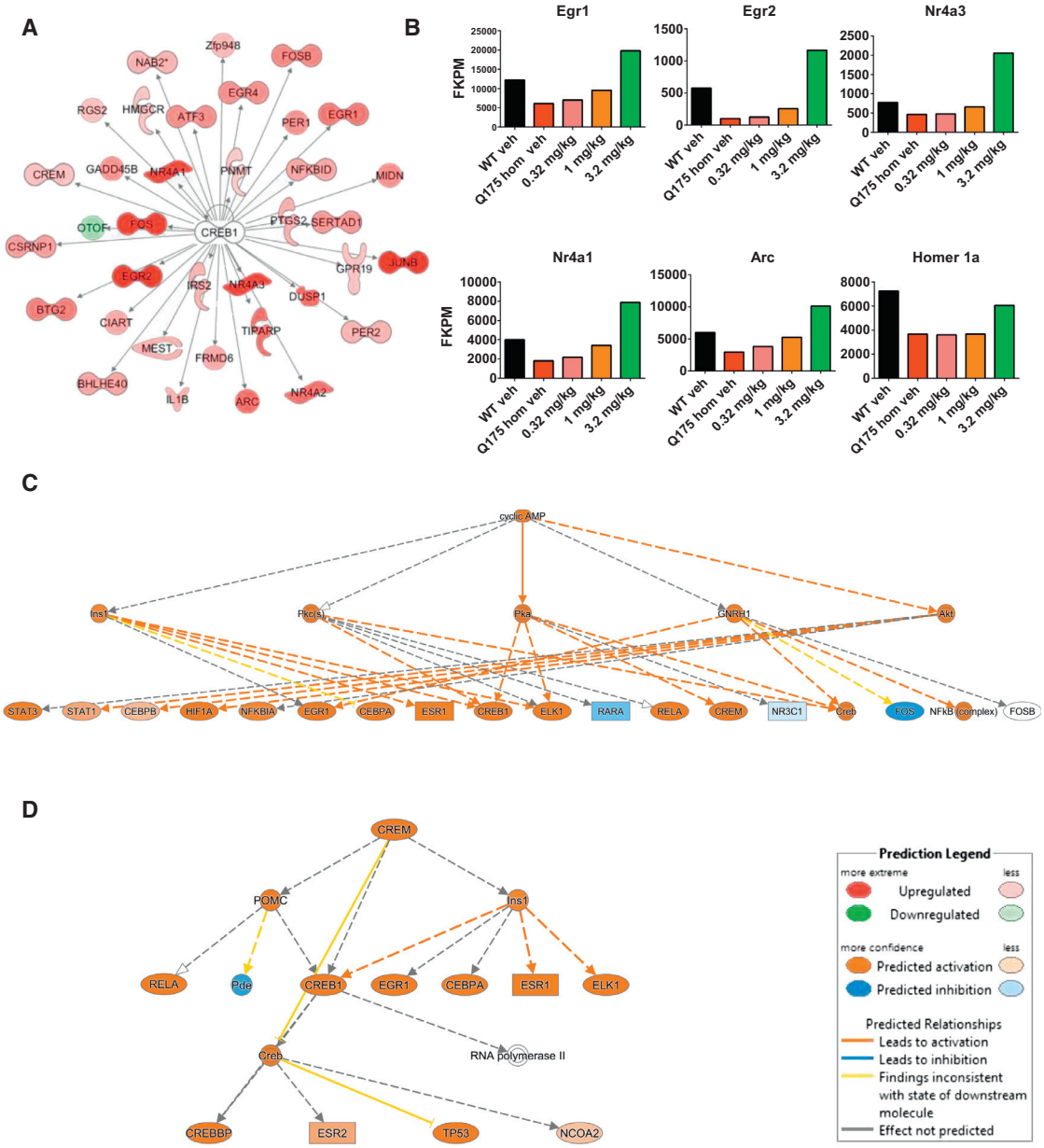

Figure 8. Chronic PDE10i Treatment Results in Activation of CREB-, CREM-, and cAMP-Mediated Transcriptional Responses in Q175 Hom Mice

(A) Proximal network of genes regulated by CREB1 in Q175 mice following chronic PF-920 treatment (3.2 mg/kg).

(B) Selected IEGs showing expression levels in WT and Q175 hom mice treated with vehicle or PF-920.

(C) Mechanistic network reconstructed from IPA upstream analysis module for the cAMP related network. The activation states of the proteins predicted from the mRNA levels are shown in orange and blue.

(D) Mechanistic network reconstructed from IPA upstream analysis module for the CREM related network. The coloring is the same as in (C) above.

including Dusp1, −2, −6, and −14 (Table S7). This was consistent with the phospho-proteomic analysis.

We independently verified the effects of treatment in a subset of genes using the Nanostring nCounter system (Table S7), which confirmed expression differences for 70% (140/201 genes), including those with differences as low as 1.2-fold. For genes whose expression was >50 fragments per kilobase per million (FPKM), the confirmation rate was over 95% (90/94).

128 striatal transcripts differentially expressed in Q175 hom showed significant rescue after treatment (Table S7). The cJun/AP-1 transcription factor complex and the expression of IEGs were a hallmark of these rescues. IEG and activity-dependent genes were strongly modulated by PDE10i, including Egr 1,

2, 3, and 4, Arc, inhibin B, Atf3, homer1a, Nr4a1, Nr4a2, and Nr4a3 (2- to 11-fold induction; Table S7; Figure 8B), indicative of the modulation of programs implicated in neuronal excitability, synaptic plasticity, and neuronal survival (Sgambato et al., 1998). Additionally, transcripts downstream of the CREB1 transcription factor show rescue (Figure 8A; $p = 1.3 \times 10^{-28}$). CREM (Figure 8D; $p = 2.7 \times 10^{-32}$) and BDNF ($p = 1.7 \times 10^{-10}$) target genes also show significant signs of rescue.

In the cortex, n = 585 genes were responsive to treatment in a dose-dependent manner, with n = 33 showing a statistical sign of rescue (Table S7).

DISCUSSION

R6/2 and Q175 HD model mice faithfully replicate PDE10 loss to an extent equivalent to that reported in manifest HD patients. Decline in PDE10 enzyme begins early in disease course, mirroring findings observed in HDGECs before disease onset (Russell et al., 2014). Despite loss of expression of PDE10 in symptomatic HD mice, PDE10 inhibitors are still effective in meaningfully raising striatal cAMP and cGMP, acutely eliciting multiple phosphostate changes of striatal proteins in symptomatic HD models. This is encouraging in anticipating HD patient responsiveness to PDE10i despite enzyme loss in patients.

PDE10 loss in HD models was not accompanied by a significant alteration in basal striatal cAMP and cGMP levels compared to WT, suggesting loss of PDE10 may be balanced by alterations in cyclic nucleotide generation. This finding was reiterated in the phosphoproteomic analysis, where we did not identify significant phosphosite changes between WT, Q175 het, and hom vehicle-treated mice. In this respect, we found ADCY5 loss tightly correlated to both PDE1 and PDE10 loss in Q175 mice. This deserves further attention in the context of HD pathology: recently, a loss of function mutation of ADCY5 was shown to be the cause of autosomal dominant chorea and dystonia (Carapito et al., 2014) and gain of function mutations leading to familial dyskinesia have been identified (Chen et al., 2014).

In symptomatic HD mouse models, acute PDE10 inhibition reversed SPN hyperexcitability in in vitro slice preparations and restored hippocampal LTP deficits in vitro in R6/2 mice, and, that despite PDE10 loss, PDE10 inhibition was still capable of increasing pathologically diminished corticostriatal input and IP activity acutely in vivo. The ex vivo evaluations support the notion that cyclic nucleotide dysregulation is a component underlying HD neurophysiological dysfunction. In addition to elevating cAMP, our additional data show that restoration of cGMP signaling is an important component to the beneficial effects of PDE10i. Neurophysiological effects of cGMP in response to PDE inhibition are becoming more appreciated (Nagy et al., 2015; Padovan-Neto et al., 2015; Saavedra et al., 2013; Zhu et al., 2016).

The phosphoproteomic study was conducted with the primary aim of identifying the neural substrates underlying the acute beneficial actions of PDE10i. Our ex vivo evaluation of improvement in corticostriatal transmission indicated the potential contribution of a pre-synaptic component to this effect (reduced PPR), although the more robust activation of the corticostriatal pathway seen in vivo in both WT and Q175 models suggests additional mechanisms. We detected robust phospho-regulation at multiple sites of glutamate and GABA receptors, their associated scaffolding proteins and ion channels that would be expected to acutely affect neurophysiological function, suggesting that the effect of PDE10i in vivo where all signaling pathways leading to activation of cAMP and cGMP are intact is more complex than seen in slices. This data set now provides valuable information that can be mined to further inform detailed molecular interrogation of the role of PDE10 in regulating striatal excitability, both in WT mice and HD models. As expected, in vivo, we did also find robust evidence of CREB pathway activation and MAP kinase signaling cascades in WT mice which were still present, if attenuated, in symptomatic Q175 mice.

Compared to the modulation of protein phosphorylation by cAMP signaling, there is less known about phospho-regulation of proteins in response to cGMP signaling cascades. Nitric oxide synthase (NOS) expression is downregulated in symptomatic R6/2 mice, in addition to CAMKIV, which can alter NOS activity and subsequent cGMP signaling through guanylate cyclase activation by alteration of the phosphorylation state of NOS at S847 (Deckel et al., 2001). Changes in NOS levels were not detected in our study, but we did detect a significant reduction in CAMKIV levels in Q175 (Table S3).

Regarding further possible evidence of cGMP signaling deregulation in HD models, the increase in HAP1 levels in Q175 mice are intriguing. In situ hybridization studies show HAP1 and neuronal NOS mRNA localization closely resemble each other, and immunocytochemical studies show co-localization of HAP1 with nNOS in rat brain (Li et al., 1996). Given the more avid association of HAP-1 to mHTT, these authors speculated a role of NO signaling in HD. HAP1 is a cGMP-dependent kinase anchoring protein (GKAP), specific for the cGMP-dependent protein kinase 1 β isoform (PKRG1) (Corradini et al., 2015), providing a rationale whereby altered mHTT-HAP1-PKRG1 complexes could potentially influence cGMP-dependent target phosphorylation by changing spatio-temporal cGMP signaling in HD.

HD models have been extensively characterized behaviorally and at a molecular level, but there remains a paucity of knowledge about HD basal ganglia dysfunction at a neurophysiological or circuitry level, beyond interrogation of corticostriatal and SPN dysfunction. We have extended the neurophysiological phenotyping of the Q175 KI model, with a focus first on evaluation of IP dysfunction. This was done primarily to translate to the human condition, where early IP dysfunction may be responsible for hyperkinetic symptom manifestation. In HD models, we believe that this selective/temporally spaced impairment of the IP compared to DP may not be well recapitulated, whereby the models may better reflect JHD, being predominantly hypo-kinesic. We show that in addition to corticostriatal and SPN deficits, this model at an early symptomatic age in vivo displays an impairment of GP firing rate fidelity (Q175 hom), spontaneous STN firing rate hypo-function (het and hom), and deficient cortical activation of the IP at the level of STN responsiveness. These results were gathered under anesthesia, which can affect firing rates in vivo; thus, there would be benefit in conducting these experiments in awake, behaving, mice in the future. Despite this caveat, genotype differences are clearly apparent

and consistent with a hypo-functioning IP, which may arise both from blunted iSPN output and from other pathology within the downstream GP and STN. Because Htt/mHtt is expressed in every cell, the concept that circuit dysfunction arises only from cortico-striatal or iSPN atrophy contributing to IP dysfunction in HD patients (and models) should be questioned (Lange et al., 1976; Waldvogel et al., 2015). In Q175 mice, we have extended this primary pathology to also implicate a hypo-functioning "hyperdirect" cortico-STN pathway, which could also contribute to hyperkinesic symptom manifestation. The gaps in our knowledge of HD basal ganglia dysfunction are still manifest; however, at this point, we provide convincing evidence of deficient IP output in HD models, and IP activation at the level of corticostriatal and STN functional improvement by PDE10i administration in a HD context; a presumed highly desirable therapeutic goal.

Finally, we show that chronic treatment of Q175 mice with PDE10i starting at pre-symptomatic ages mitigates the emergence of mHTT-induced corticostriatal transmission deficits and, to a variable extent, aberrant SPN excitability. Our RNA-sequencing (seq) and phospho-proteome analyses suggest numerous mechanisms by which both acute and chronic PDE10i may be beneficial. Modulation of CREB and ERK signaling affects striatal gene expression (Kleiman et al., 2011; Strick et al., 2010), and deficiency in both pathways have been implicated in HD (Bodai and Marsh, 2012; Roze et al., 2008) and associated with neurodegeneration (Jancic et al., 2009; Mantamadiotis et al., 2002). Our data corroborate upregulation of CREB, CREM, and now, cJun/AP-1-mediated transcription in HD model striatum by PDE10i. IEG and activity-dependent gene expression control both neuronal excitability and plasticity mechanisms in SPNs (Flavell and Greenberg, 2008; Sgambato et al., 1998; Spektor et al., 2002). These effects could arise from a cell-autonomous response to blocking PDE10 in SPNs or also involve signaling via enhanced cortical-driven afferent input.

On the basis of this data, clinical trials of PF-02545920 to assess symptom improvement in manifest HD patients are underway. This trial is based on the notion that preferentially boosting corticostriatal transmission and IP activity can provide amelioration of adult HD symptoms. The outcome of this trial will be invaluable to inform both the pre-clinical and clinical HD research community on the "translational predictiveness" of the pre-clinical validation approach we chose to undertake.

EXPERIMENTAL PROCEDURES

Q175 mice (JAX strain name: B6.129S1-Htttm1Mfc/190JChdi; CHDI-81003003) and R6/2 mice (JAX strain name: B6CBA-Tg(HDexon1)62Gpb/125JChdi; CHDI-81001000) were used throughout this study. See Supplemental Experimental Procedures for further details. Detailed information on statistical tests performed and statistical results are shown in Table S8. Figures and text are annotated with significance as follows: ns = non-significant, (# = p = 0.06–0.07); * = $p < 0.05$, ** = $p < 0.01$, *** = $p < 0.001$; and **** = $p < 0.0001$.

All animal care and in vivo procedures conducted at Pfizer Inc. were approved by the Pfizer Animal Care and Use Committee and conducted in accordance with the guide for the Care and Use of Laboratory Animals (Institute of Laboratory Animal Resources, 1996).

For microPET studies, animals were housed at the animal department of Karolinska University Hospital, Stockholm, Sweden and all experiments were performed in accordance with the guidelines of the Swedish National Board of Laboratory Animals under protocols approved by the Animal Ethics Review Board of Northern Stockholm, Sweden (N558/11).

Animal procedures were approved by the Institutional Animal Care and Use Committee of Rosalind Franklin University of Medicine and Science, and of Psychogenics, Inc. (PHS OLAW animal welfare assurance number A4471-01), an AAALAC International accredited institution (Unit #001213).

Animal experiments at Charles River were conducted according to the National Institute of Health (NIH) guidelines for the care and use of laboratory animals, and approved by the State Provincial Office of Southern Finland.

ACCESSION NUMBERS

The accession numbers for the RNA-sequencing data and quantitative proteome and phosphoproteome analysis reported in this paper are GEO: GSE89505 and PRIDE: PXD005138, respectively.

SUPPLEMENTAL INFORMATION

Supplemental Information includes Supplemental Experimental Procedures, eight figures, and eight tables and can be found with this article online at http://dx.doi.org/10.1016/j.neuron.2016.10.064.

A video abstract is available at http://dx.doi.org/10.1016/j.neuron.2016.10.064#mmc9.

AUTHOR CONTRIBUTIONS

J.F.H., K.M.W., and (C.J.S.) performed and analyzed pharmacodynamic experiments in Figure 1. S.Z., H.L., W.J.X., F.E.P.-N., S.C., (A.G., and A.R.W.) performed and analyzed in vivo electrophysiology. A.B., E.S., M.G., K.W., (B.B., and V.B.) performed and analyzed ex vivo electrophysiology. J.H., M.T., (A.V., C.H., and L.M.) performed and analyzed microPET experiments. J.N.D., S.E., (C.S., and D.L.) performed and analyzed proteomic experiments and (K.L., T.H., and L.P.) coordinated in vivo dosing, behavior, and MRI. J.R. analyzed RNA-seq data. J.B., M.K., and (A.G.) conducted qPCR. Authors in parentheses provided scientific direction and managerial oversight. V.B., I.M.-S., M.M.Z., and C.J.S. designed the testing paradigm for evaluation of PDE10i for HD. V.B. coordinated research activities and V.B. and I.M.-S. wrote the paper.

ACKNOWLEDGMENTS

We thank CRL Finland technicians for animal dosing, Dr. Jennifer Ware for statistical advice, Dr. Martina Blumenthal for administrative help, and Drs. D. James Surmeier, Mark Bevan, and Simon Noble for their review of the manuscript. Studies were funded by CHDI Foundation, Inc. and Pfizer, Inc. J.F.H., K.M.W., M.M.Z., and C.J.S. are Pfizer employees. PF-02545920 is owned by Pfizer, Inc. and is in a clinical trial to evaluate its effectiveness for therapeutic benefit in HD. C.J.S., K.M.W., J.F.H., and M.M.Z. are employees of Pfizer.

Received: April 8, 2016
Revised: September 14, 2016
Accepted: October 23, 2016
Published: December 1, 2016

REFERENCES

Ahmad, R., Bourgeois, S., Postnov, A., Schmidt, M.E., Bormans, G., Van Laere, K., and Vandenberghe, W. (2014). PET imaging shows loss of striatal PDE10A in patients with Huntington disease. Neurology *82*, 279–281.

Albin, R.L., Reiner, A., Anderson, K.D., Dure, L.S., 4th, Handelin, B., Balfour, R., Whetsell, W.O., Jr., Penney, J.B., and Young, A.B. (1992). Preferential loss of striato-external pallidal projection neurons in presymptomatic Huntington's disease. Ann. Neurol. *31*, 425–430.

Alexandrov, V., Brunner, D., Menalled, L.B., Kudwa, A., Watson-Johnson, J., Mazzella, M., Russell, I., Ruiz, M.C., Torello, J., Sabath, E., et al. (2016).

Large-scale phenome analysis defines a behavioral signature for Huntington's disease genotype in mice. Nat. Biotechnol. *34*, 838–844.

Beaumont, V., Park, L., Rassoulpour, A., Dijkman, U., Heikkinen, T., Lehtimaki, K., Kontkanen, O., Al Nackkash, R., Bates, G.P., Gleyzes, M., et al. (2014). The PDE1/5 inhibitor SCH-51866 does not modify disease progression in the R6/2 mouse model of Huntington's disease. PLoS Curr. *6*, 6.

Biglan, K.M., Zhang, Y., Long, J.D., Geschwind, M., Kang, G.A., Killoran, A., Lu, W., McCusker, E., Mills, J.A., Raymond, L.A., et al.; PREDICT-HD Investigators of the Huntington Study Group (2013). Refining the diagnosis of Huntington disease: the PREDICT-HD study. Front. Aging Neurosci. *5*, 12.

Bodai, L., and Marsh, J.L. (2012). A novel target for Huntington's disease: ERK at the crossroads of signaling. The ERK signaling pathway is implicated in Huntington's disease and its upregulation ameliorates pathology. BioEssays *34*, 142–148.

Carapito, R., Paul, N., Untrau, M., Le Gentil, M., Ott, L., Alsaleh, G., Jochem, P., Radosavljevic, M., Le Caignec, C., David, A., et al. (2014). A De Novo ADCY5 mutation causes early-onset autosomal dominant chorea and dystonia. Mov. Disord. http://dx.doi.org/10.1002/mds.26115.

Chen, Y.Z., Friedman, J.R., Chen, D.H., Chan, G.C., Bloss, C.S., Hisama, F.M., Topol, S.E., Carson, A.R., Pham, P.H., Bonkowski, E.S., et al. (2014). Gain-of-function ADCY5 mutations in familial dyskinesia with facial myokymia. Ann. Neurol. *75*, 542–549.

Corradini, E., Burgers, P.P., Plank, M., Heck, A.J., and Scholten, A. (2015). Huntingtin associated protein (HAP1) is a cGMP-dependent kinase anchoring protein (GKAP), specific for the cGMP-dependent protein kinase Ibeta isoform. J. Biol. Chem. *290*, 7887–7896.

Deckel, A.W., Gordinier, A., Nuttal, D., Tang, V., Kuwada, C., Freitas, R., and Gary, K.A. (2001). Reduced activity and protein expression of NOS in R6/2 HD transgenic mice: effects of L-NAME on symptom progression. Brain Res. *919*, 70–81.

Deng, Y.P., Albin, R.L., Penney, J.B., Young, A.B., Anderson, K.D., and Reiner, A. (2004). Differential loss of striatal projection systems in Huntington's disease: a quantitative immunohistochemical study. J. Chem. Neuroanat. *27*, 143–164.

Doig, N.M., Moss, J., and Bolam, J.P. (2010). Cortical and thalamic innervation of direct and indirect pathway medium-sized spiny neurons in mouse striatum. J. Neurosci. *30*, 14610–14618.

Eidelberg, D., and Surmeier, D.J. (2011). Brain networks in Huntington disease. J. Clin. Invest. *121*, 484–492.

Flavell, S.W., and Greenberg, M.E. (2008). Signaling mechanisms linking neuronal activity to gene expression and plasticity of the nervous system. Annu. Rev. Neurosci. *31*, 563–590.

Giampà, C., Laurenti, D., Anzilotti, S., Bernardi, G., Menniti, F.S., and Fusco, F.R. (2010). Inhibition of the striatal specific phosphodiesterase PDE10A ameliorates striatal and cortical pathology in R6/2 mouse model of Huntington's disease. PLoS ONE *5*, e13417.

Giralt, A., Saavedra, A., Carretón, O., Arumí, H., Tyebji, S., Alberch, J., and Pérez-Navarro, E. (2013). PDE10 inhibition increases GluA1 and CREB phosphorylation and improves spatial and recognition memories in a Huntington's disease mouse model. Hippocampus *23*, 684–695.

The Huntington's Disease Collaborative Research Group (1993). A novel gene containing a trinucleotide repeat that is expanded and unstable on Huntington's disease chromosomes. Cell *72*, 971–983.

Heikkinen, T., Lehtimäki, K., Vartiainen, N., Puoliväli, J., Hendricks, S.J., Glaser, J.R., Bradaia, A., Wadel, K., Touller, C., Kontkanen, O., et al. (2012). Characterization of neurophysiological and behavioral changes, MRI brain volumetry and 1H MRS in zQ175 knock-in mouse model of Huntington's disease. PLoS ONE *7*, e50717.

Herdegen, T., and Leah, J.D. (1998). Inducible and constitutive transcription factors in the mammalian nervous system: control of gene expression by Jun, Fos and Krox, and CREB/ATF proteins. Brain Res. Brain Res. Rev. *28*, 370–490.

Jancic, D., Lopez de Armentia, M., Valor, L.M., Olivares, R., and Barco, A. (2009). Inhibition of cAMP response element-binding protein reduces neuronal excitability and plasticity, and triggers neurodegeneration. Cereb. Cortex *19*, 2535–2547.

Kavalali, E.T., Chung, C., Khvotchev, M., Leitz, J., Nosyreva, E., Raingo, J., and Ramirez, D.M. (2011). Spontaneous neurotransmission: an independent pathway for neuronal signaling? Physiology (Bethesda) *26*, 45–53.

Kleiman, R.J., Kimmel, L.H., Bove, S.E., Lanz, T.A., Harms, J.F., Romegialli, A., Miller, K.S., Willis, A., des Etages, S., Kuhn, M., and Schmidt, C.J. (2011). Chronic suppression of phosphodiesterase 10A alters striatal expression of genes responsible for neurotransmitter synthesis, neurotransmission, and signaling pathways implicated in Huntington's disease. J. Pharmacol. Exp. Ther. *336*, 64–76.

Kolomiets, B.P., Deniau, J.M., Mailly, P., Ménétrey, A., Glowinski, J., and Thierry, A.M. (2001). Segregation and convergence of information flow through the cortico-subthalamic pathways. J. Neurosci. *21*, 5764–5772.

Lange, H., Thörner, G., Hopf, A., and Schröder, K.F. (1976). Morphometric studies of the neuropathological changes in choreatic diseases. J. Neurol. Sci. *28*, 401–425.

Letort, D., and Gonzalez-Alegre, P. (2013). Huntington's disease in children. Handb. Clin. Neurol. *113*, 1913–1917.

Li, X.J., Sharp, A.H., Li, S.H., Dawson, T.M., Snyder, S.H., and Ross, C.A. (1996). Huntingtin-associated protein (HAP1): discrete neuronal localizations in the brain resemble those of neuronal nitric oxide synthase. Proc. Natl. Acad. Sci. USA *93*, 4839–4844.

Mantamadiotis, T., Lemberger, T., Bleckmann, S.C., Kern, H., Kretz, O., Martin Villalba, A., Tronche, F., Kellendonk, C., Gau, D., Kapfhammer, J., et al. (2002). Disruption of CREB function in brain leads to neurodegeneration. Nat. Genet. *31*, 47–54.

Matsuoka, I., Suzuki, Y., Defer, N., Nakanishi, H., and Hanoune, J. (1997). Differential expression of type I, II, and V adenylyl cyclase gene in the postnatal developing rat brain. J. Neurochem. *68*, 498–506.

Miller, B.R., Walker, A.G., Shah, A.S., Barton, S.J., and Rebec, G.V. (2008). Dysregulated information processing by medium spiny neurons in striatum of freely behaving mouse models of Huntington's disease. J. Neurophysiol. *100*, 2205–2216.

Miller, B.R., Walker, A.G., Barton, S.J., and Rebec, G.V. (2011). Dysregulated neuronal activity patterns implicate corticostriatal circuit dysfunction in multiple rodent models of Huntington's disease. Front. Syst. Neurosci. *5*, 26.

Nagy, D., Tingley, F.D., 3rd, Stoiljkovic, M., and Hajós, M. (2015). Application of neurophysiological biomarkers for Huntington's disease: evaluating a phosphodiesterase 9A inhibitor. Exp. Neurol. *263*, 122–131.

Nelson, A.B., and Kreitzer, A.C. (2014). Reassessing models of basal ganglia function and dysfunction. Annu. Rev. Neurosci. *37*, 117–135.

Nishi, A., Kuroiwa, M., Miller, D.B., O'Callaghan, J.P., Bateup, H.S., Shuto, T., Sotogaku, N., Fukuda, T., Heintz, N., Greengard, P., and Snyder, G.L. (2008). Distinct roles of PDE4 and PDE10A in the regulation of cAMP/PKA signaling in the striatum. J. Neurosci. *28*, 10460–10471.

Padovan-Neto, F.E., Sammut, S., Chakroborty, S., Dec, A.M., Threlfell, S., Campbell, P.W., Mudrakola, V., Harms, J.F., Schmidt, C.J., and West, A.R. (2015). Facilitation of corticostriatal transmission following pharmacological inhibition of striatal phosphodiesterase 10A: role of nitric oxide-soluble guanylyl cyclase-cGMP signaling pathways. J. Neurosci. *35*, 5781–5791.

Plotkin, J.L., and Surmeier, D.J. (2015). Corticostriatal synaptic adaptations in Huntington's disease. Curr. Opin. Neurobiol. *33*, 53–62.

Reedeker, N., Van Der Mast, R.C., Giltay, E.J., Van Duijn, E., and Roos, R.A. (2010). Hypokinesia in Huntington's disease co-occurs with cognitive and global dysfunctioning. Mov. Disord. *25*, 1612–1618.

Roze, E., Betuing, S., Deyts, C., Marcon, E., Brami-Cherrier, K., Pagès, C., Humbert, S., Mérienne, K., and Caboche, J. (2008). Mitogen- and stress-activated protein kinase-1 deficiency is involved in expanded-huntingtin-induced transcriptional dysregulation and striatal death. FASEB J. *22*, 1083–1093.

Russell, D.S., Barret, O., Jennings, D.L., Friedman, J.H., Tamagnan, G.D., Thomae, D., Alagille, D., Morley, T.J., Papin, C., Papapetropoulos, S., et al. (2014). The phosphodiesterase 10 positron emission tomography tracer, [18F]MNI-659, as a novel biomarker for early Huntington disease. JAMA Neurol. *71*, 1520–1528.

Saavedra, A., Giralt, A., Arumí, H., Alberch, J., and Pérez-Navarro, E. (2013). Regulation of hippocampal cGMP levels as a candidate to treat cognitive deficits in Huntington's disease. PLoS ONE *8*, e73664.

Sgambato, V., Pagès, C., Rogard, M., Besson, M.J., and Caboche, J. (1998). Extracellular signal-regulated kinase (ERK) controls immediate early gene induction on corticostriatal stimulation. J. Neurosci. *18*, 8814–8825.

Siuciak, J.A., Chapin, D.S., Harms, J.F., Lebel, L.A., McCarthy, S.A., Chambers, L., Shrikhande, A., Wong, S., Menniti, F.S., and Schmidt, C.J. (2006). Inhibition of the striatum-enriched phosphodiesterase PDE10A: a novel approach to the treatment of psychosis. Neuropharmacology *51*, 386–396.

Spektor, B.S., Miller, D.W., Hollingsworth, Z.R., Kaneko, Y.A., Solano, S.M., Johnson, J.M., Penney, J.B., Jr., Young, A.B., and Luthi-Carter, R. (2002). Differential D1 and D2 receptor-mediated effects on immediate early gene induction in a transgenic mouse model of Huntington's disease. Brain Res. Mol. Brain Res. *102*, 118–128.

Strick, C.A., James, L.C., Fox, C.B., Seeger, T.F., Menniti, F.S., and Schmidt, C.J. (2010). Alterations in gene regulation following inhibition of the striatum-enriched phosphodiesterase, PDE10A. Neuropharmacology *58*, 444–451.

Tabrizi, S.J., Scahill, R.I., Owen, G., Durr, A., Leavitt, B.R., Roos, R.A., Borowsky, B., Landwehrmeyer, B., Frost, C., Johnson, H., et al.; TRACK-HD Investigators (2013). Predictors of phenotypic progression and disease onset in premanifest and early-stage Huntington's disease in the TRACK-HD study: analysis of 36-month observational data. Lancet Neurol. *12*, 637–649.

Threlfell, S., Sammut, S., Menniti, F.S., Schmidt, C.J., and West, A.R. (2009). Inhibition of phosphodiesterase 10A increases the responsiveness of striatal projection neurons to cortical stimulation. J. Pharmacol. Exp. Ther. *328*, 785–795.

Traynelis, S.F., Wollmuth, L.P., McBain, C.J., Menniti, F.S., Vance, K.M., Ogden, K.K., Hansen, K.B., Yuan, H., Myers, S.J., and Dingledine, R. (2010). Glutamate receptor ion channels: structure, regulation, and function. Pharmacol. Rev. *62*, 405–496.

Unschuld, P.G., Joel, S.E., Liu, X., Shanahan, M., Margolis, R.L., Biglan, K.M., Bassett, S.S., Schretlen, D.J., Redgrave, G.W., van Zijl, P.C., et al. (2012). Impaired cortico-striatal functional connectivity in prodromal Huntington's Disease. Neurosci. Lett. *514*, 204–209.

van den Bogaard, S.J., Dumas, E.M., Acharya, T.P., Johnson, H., Langbehn, D.R., Scahill, R.I., Tabrizi, S.J., van Buchem, M.A., van der Grond, J., and Roos, R.A.; TRACK-HD Investigator Group (2011). Early atrophy of pallidum and accumbens nucleus in Huntington's disease. J. Neurol. *258*, 412–420.

Waldvogel, H.J., Kim, E.H., Tippett, L.J., Vonsattel, J.P., and Faull, R.L. (2015). The neuropathology of Huntington's disease. Curr. Top. Behav. Neurosci. *22*, 33–80.

Zhu, J., Shang, Y., and Zhang, M. (2016). Mechanistic basis of MAGUK-organized complexes in synaptic development and signalling. Nat. Rev. Neurosci. *17*, 209–223.